

Review

Magnetic Semiconductors as Materials for Spintronics

Andrei Telegin ^{1,2,*}  and Yurii Sukhorukov ¹¹ Nanospintronics Department, IMP UB RAS, Yekaterinburg 620108, Russia² Department of Physics, UNIST, Ulsan 44919, Republic of Korea

* Correspondence: andrei@unist.ac.kr or telegin@imp.uran.ru; Tel.: +7-343-374-5244

Abstract: From the various aspects of spintronics the review highlights the area devoted to the creation of new functional materials based on magnetic semiconductors and demonstrates both the main physical phenomena involved and the technical possibilities of creating various devices: maser, p-n diode with colossal magnetoresistance, spin valve, magnetic lens, optical modulators, spin wave amplifier, etc. Particular attention is paid to promising research directions such as ultrafast spin transport and THz spectroscopy of magnetic semiconductors. Special care has been taken to include a brief theoretical background and experimental results for the new spintronics approach employing magnetostrictive semiconductors—strain-magneto-optics. Finally, it presents top-down approaches for magnetic semiconductors. The mechano-physical methods of obtaining and features of the physical properties of high-density nanoceramics based on complex magnetic oxides are considered. The potential possibility of using these nanoceramics as an absorber of solar energy, as well as in modulators of electromagnetic radiation, is shown.

Keywords: spintronics; magnetic semiconductors; complex magnetic oxides; ferrite spinel; colossal magnetoresistance; nanoceramics; thin-film structures; maser; modulator; optoelectronics

**Citation:** Telegin, A.; Sukhorukov, Y.

Magnetic Semiconductors as

Materials for Spintronics.

Magnetochemistry **2022**, *8*, 173.[https://doi.org/10.3390/](https://doi.org/10.3390/magnetochemistry8120173)[magnetochemistry8120173](https://doi.org/10.3390/magnetochemistry8120173)

Academic Editor: Yuan-Chieh

Tseng

Received: 31 October 2022

Accepted: 23 November 2022

Published: 29 November 2022

Publisher's Note: MDPI stays neutral with regard to jurisdictional claims in published maps and institutional affiliations.



Copyright: © 2022 by the authors. Licensee MDPI, Basel, Switzerland. This article is an open access article distributed under the terms and conditions of the Creative Commons Attribution (CC BY) license (<https://creativecommons.org/licenses/by/4.0/>).

1. Introduction

A magnetic semiconductor is a magnetic material that, in terms of specific conductivity, occupies an intermediate position between a conductor and an insulator, and has a band gap comparable to $\sim k_B T$. Most known magnetic semiconductors (SC) are either oxides or chalcogenides (sulfides, selenides and tellurides) of 3d transition metals, rare earth 4f metals or a combination. The strong interaction of mobile charge carriers with the localized magnetic moments of the d- and f-shells leads to a number of features of the electrical and optical properties of magnetic SC that are absent in non-magnetic semiconductor [1–9].

There are several properties typical only for magnetic SC. For example, in ferromagnetic semiconductors (europium chalcogenides, chromium chalcogenide spinel, etc.), with either a decrease in temperature, application of an external magnetic field or both, a giant (up to ~ 0.5 eV) shift towards long wavelengths of the edge of optical absorption and photoconductivity is observed, the so-called giant red shift of the absorption edge. Meanwhile, near the Curie temperature they can exhibit a colossal magnetoresistance (CMR) effect and a metal-insulator (MI) transition. Giant magneto-optical (MO) effects were found in magnetic SCs in a wide visible and infrared (IR) spectral range (Faraday and Kerr effects, magnetotransmission, magnetoreflexion, magnetic linear and circular dichroism, etc.) [10–14]. Moreover, magnetic SCs are the basis of high-temperature superconductors and without considering the properties of magnetic semiconductors, it would be impossible to construct a theory of high temperature superconductivity (HTSC). By changing the concentration of current carriers (by temperature, doping, light irradiation, application of electric field, current injection, etc.), it is possible to easily change the magnetic properties of SCs [1–7,15–20]. On the contrary, their electrical and optical properties can be controlled by an external magnetic field, which in relation to the intense development of electronics and magnetophotonics is of high practical interest [21–25]. For example, the

presence of a large magnetocaloric effect in manganites makes magnetic SCs promising materials for creating refrigerators [26]. Large MO effects and the presence of the MI transition in magnetic oxides made it possible to create a wide range of optoelectronic devices, such as modulators, magnetic field visualization sensors, MO filters, shutters, attenuators, bolometers, thermochromic materials, etc. [27–33]. The electrical properties of perovskites and cobaltites allowed for using them as cathodes in solid oxide fuel cells, opening new possibilities for creating alternative energy sources with a high efficiency of ~90% [34,35]. The medical direction of using magnetic SCs is also very important, for example, as a material for artificial local heating of a selected area of the body-hyperthermia [36–40].

Unlike non-magnetics, magnetic semiconductors have the important property of dependence of the band structure on the orientation of the electron spin. In other words, in magnetic SCs, the band gap is not the same for electrons with different spin orientations (Figure 1).

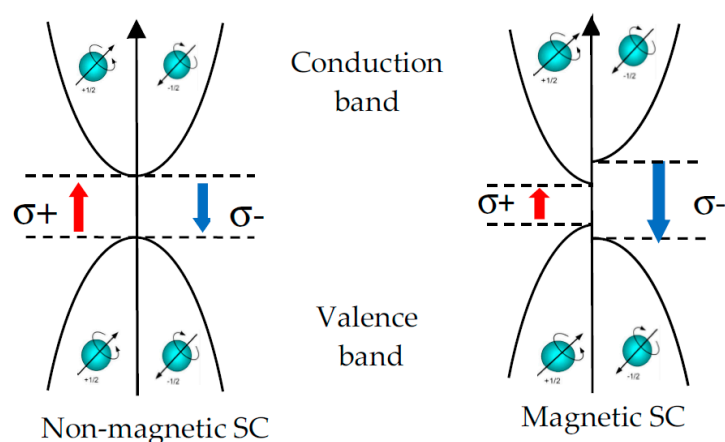


Figure 1. Schematic representation of changes in the band structure of a magnetic SCs depending on the orientation of the electron spin (right), which are absent in the band structure of a non-magnetic semiconductor (left).

The presence of bands with different orientations of the of charge carriers' spins (spin-polarized bands) made it possible to control the charge current in magnetic SCs, depending on the mutual orientation of the magnetic field, current direction and an applied voltage. It is important that the flow of spin-oriented (spin-polarized) charged particles retains its properties not only in magnetic SCs, but also in other magnetic or non-magnetic media at a sufficiently level. In non-magnetic semiconductors, spins with different orientations compensate each other, thus the full spin current is zero and there is only the current of charged particles. The possibility of creating and manipulating a flow of spin-polarized charge carriers in magnetic SCs has opened broad prospects for creating new functional materials and various electronic devices. Spintronics (spin electronics) studies spin current transfer (spin-polarized transport) in condensed media, including contact structures, heterostructures, superlattices and multilayers. In all these cases, the source of spin-polarized electrons (spin injector) is a ferromagnet (metal or semiconductor), which in the magnetized state has the spontaneous spin ordering of the current carriers [15–25]. In ferromagnetic SCs, the levels of spin polarization can reach higher values (up to almost 100%) than in metals (up to 10%) [41]. In non-magnetic SCs in an external magnetic field, the Zeeman splitting of the conduction band occurs with the formation of two energy sublevels. When spin-polarized electrons are injected from a magnetic SC into a non-magnetic SC, controlled transitions to both the upper and lower energy levels become possible, which allows controlling the charge current by an external influence. This area of physics has been intensively developed over the past 30 years [42–49].

At the same time, current spintronic devices or their components are generally extremely small ($\sim 10^{-7}$ m) and can be classified as nanomaterials. When the dimensions of device components or a material are reduced to a nanometer scale (for example, films, thin-

film structures, fibers, powders and high-density ceramics), their mechanical properties are changed significantly, thermal conductivity is increased and a change of fundamental characteristics such as the melting temperature and Debye temperature were also reported. In a magnetic SC, during the transition to the nanoscale, the electronic structure is drastically changed followed by the appearance of various anomalies in its magnetic and transport properties [50,51]. This paper presents a brief overview of the experimental results and technical solutions obtained in the field of spintronics based on the spin-dependent phenomena in bulk crystals, thin films, heterostructures and nanoceramics of magnetic semiconductors.

2. Functional Materials and Devices Promising for Spintronics Based on Magnetic Semiconductors

2.1. Heterostructures FM/SC

Modern technology and electronics implement almost the entire range of electromagnetic radiation from ultra-long waves of hundreds of kilometers to very short waves of the nanometer range. As a source of electromagnetic waves, various electrovacuum and semiconductor, heating and gas-discharge devices and solid-state structures, such as LEDs, lasers, etc., are often used. However, there is a poorly studied part of the spectrum in the wavelength range from ~ 1 to 0.1 mm due to the absence of natural sources and receivers of electromagnetic radiation for this spectral range.

In 1989, after the discovery of a giant magnetoplasmon absorption in a contact structure made of a ferromagnetic (FM) semiconductor, HgCr_2Se_4 , with a high degree of polarization of charge carriers and a semiconductor, InSb [52], a new physical model was proposed for creating an electromagnetic radiation source for the millimeter and submillimeter wavelength range controlled by a magnetic field. Later, within the framework of the same model, the possibility of creating an electromagnetic radiation receiver was also substantiated [53]. The essence of the model is shown in Figure 2. Both panels show the scheme of the electron spin transitions for different FM/SC heterostructures. To obtain electromagnetic emission in such a heterostructure, two conditions must be fulfilled.

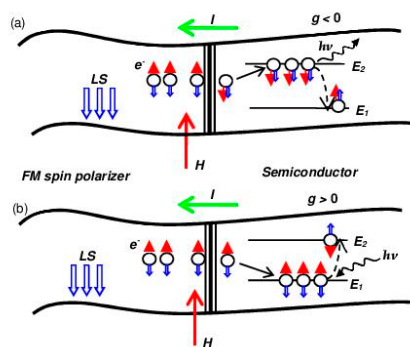


Figure 2. Schematic representation of the FM/SC heterostructure with spin-polarized electron transport from the ferromagnetic SC (a) for the case of an inverse population of the upper Zeeman level (E_2) of the non-magnetic SC with $g < 0$ by conduction electrons and subsequent radiative recombination; (b) for the case of the population of the lower Zeeman level (E_1) of the SC with $g > 0$ by conduction electrons and subsequent photoexcitation to the upper Zeeman level. Symbols H and I denote the magnetic field and current direction, respectively, while LS —spin-orbital coupling. Red and blue arrows are assigned to the direction of the spin and the magnetic moment of electrons.

The first condition is a FM with a high degree of polarization of conduction electron spins $p = (N_{\uparrow} - N_{\downarrow}) / (N_{\uparrow} + N_{\downarrow})$, where N_{\uparrow} and N_{\downarrow} are the density of states in spin-polarized subbands. The fulfillment of this condition makes it possible to implement the transport of spin-polarized electrons from FM to SC. In ferromagnetic SC below the Curie temperature (T_C), the charge carriers are spin polarized due to the exchange interaction and the value of the spin polarization is $\sim 100\%$ [23]. The second condition is a SC with a large negative g -factor (a value proportional to the gyromagnetic ratio of the electron) and high mobility of charge carriers. In such a material, the direction of the spin and the magnetic moment

of the electrons coincide. Such conditions are met by the semiconductor n-InSb, in which $g = -52$, and mobility μ is up to $10^6 \text{ cm}^2/\text{V}\cdot\text{s}$.

An external magnetic field applied to a magnetic SC interacts with electron spins and divides them into two groups: with a magnetic moment directed along the field (lower Zeeman level) and opposite to the field (upper Zeeman level). In a two-level system, when the g -factor of the SC is negative (Figure 2a), the overpopulation of the upper Zeeman level can be artificially created by the transfer of spin-polarized electrons from the injector (FM semiconductor) by means of excitation of electrons when an electric field is applied. At the same time, upon reaching a high concentration of injected spin-polarized electrons, it is possible to obtain an inverse state and electromagnetic emission with a quantum energy $h\nu = \mu_B g H$, tunable by the magnetic field H (μ_B is the Bohr magneton, h is the Planck's constant) appears.

It should be noted, typically, that conduction electrons in SCs have a positive g -factor. The positive sign of the g -factor for a negatively charged particle means that its spin and magnetic moment are aligned in opposite directions. When a magnetic field is applied in a two-level system with a positive g -factor (Figure 2b), spin-polarized electrons from the injector are transferred to the lower energy level of the SC. Therefore, excited transitions in a semiconductor are only possible with the absorption of external electromagnetic radiation.

Recently, another idea was developed to create a solid-state maser, in which the generation of microwave radiation can arise due to the injection of electrons from the spin-nonequilibrium state [54]. Figure 3 shows a schematic representation of the structure, explaining the principle of operation of such a maser. The structure consists of FM and paramagnetic (PM) layers, which are separated from each other by an insulator tunnel barrier, for example, an aluminum or magnesium oxide. The FM layer acts as a spin polarizer for the electric current, and spin-nonequilibrium carriers are injected into the PM layer. A circular polarized electromagnetic (EM) wave with an angular velocity ω propagates along the Z axis, while the clockwise or counterclockwise magnetic field of the EM wave rotates in the XY plane, depending on the polarization direction. The injected spins oriented along the Z axis begin to precess in the magnetic field of the EM wave and, depending on the direction of the electron spin and the rotation of the magnetic field in the wave, the absorption or emission of the EM waves can be obtained.

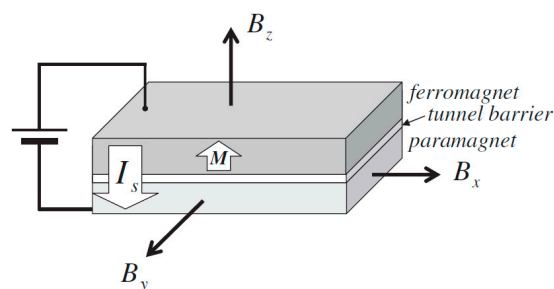


Figure 3. Schematic of an electrical spin-injection source for the paramagnetic medium. An electrical current is driven across the interface between a ferromagnetic layer and the paramagnetic layer (separated by an oxide tunnel barrier), which causes a spin current I_s to flow into the paramagnet. It is assumed that the static field B is sufficiently strong to saturate the magnetization M of the ferromagnetic layer normal to the film plane [54].

2.2. Spin Injection Maser

Semiconducting injection lasers revolutionized laser technology, utilizing them in the form of miniature devices that entered our everyday life, and gave rise to the new research direction called photonics. The first method for obtaining EM emission induced by the injection of spin-polarized electrons in a FM/SC heterostructure was presented by the Institute of Metal Physics UB of RAS, Russia [30,55]. The principle of operation of the spin-injection maser and its technical characteristics are described in detail in [56,57]. The authors showed that the most convenient materials for use as spin polarizers are magnetic

SCs, for example, $\text{EuO}_{0.98}\text{Gd}_{0.02}\text{O}$ ($T_C = 130$ K), n- and p-type HgCr_2Se_4 ($T_C = 120\text{--}130$ K), $\text{La}_{0.8}\text{Ba}_{0.2}\text{MnO}_3$ ($T_C = 280$ K), $\text{La}_{0.8}\text{Sr}_{0.2}\text{MnO}_3$ ($T_C = 308$ K) [3,30,31,58–60] and Heusler alloys Co_2MnSn ($T_C = 826$ K), Ni_2MnSn ($T_C = 340$ K) and Co_2MnSb ($T_C = 478$ K) [32,61]. A single crystal of n-InSb was used as a SC layer, which has high mobility of charge carriers, a long spin-lattice relaxation time of conduction electrons and an anomalously high absolute value of the negative g-factor of charge carriers. Figure 4 shows the real spin-injection maser device and the picture of a contact structure p- HgCr_2Se_4 /n-InSb, which does not exceed 2×2 mm² (inset of Figure 4a).

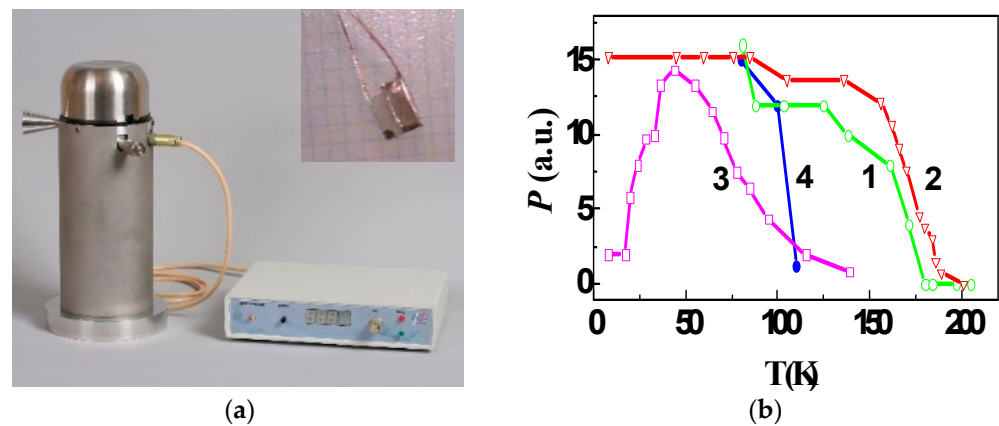


Figure 4. (a) Photo of the spin-injection maser with a control unit. Inset: the contact structure of p- HgCr_2Se_4 /n-InSb, (b) dependence of radiation power P of the maser on temperature for various contact structures: 1— Co_2MnSb /n-InSb in the field of 6 kOe and current $I = 2$ A; 2— Co_2MnSn /n-InSb at $H = 6.6$ kOe and $I = 3$ A; 3—p- HgCr_2Se_4 /n-InSb at $H = 7.5$ kOe and $I = 3$ A; 4—n- $\text{Eu}_{0.98}\text{Gd}_{0.02}\text{O}$ /n-InSb at $H = 6.2$ kOe and $I = 2$ A.

It was shown that this spin-injection maser can generate EM radiation with a power of 6–75 mW/A in the frequency range from 30 to 1500 GHz and the temperature range up to 180 K. Figure 4b demonstrates the working temperature range for various FM/SC contact structures, which is determined by the temperature of the magnetic ordering of a ferromagnet. Temperature control of the working elements is necessary for stable operation of the maser. Other aspects of FM/SC spin current transfer, which open new possibilities in solid-state electronics, can also be noted, for example, the development of theoretical aspects of amplifying EM radiation in FM/SC structures using spintronics technologies, the discovery of spin-polarized luminescence and the creation of a high-frequency diodes with output characteristics that can be controlled by an external magnetic field [38,62–64].

2.3. Amplification of Spin Waves by Drifting Charge Carriers

The coexistence of interacting subsystems of charge carriers and spin waves in a magnetic SC can lead to heating of the magnon subsystem by hot current carriers [65–67] and, as a result, to amplification of spin waves by drifting charge carriers. Electrons are heated in electric fields under FMR conditions. The electron energy received from the field is transferred to phonons and magnons. For spintronics, the effect of the amplification of spin waves by drifting charge carriers is very important. The possibility of control of the attenuation of spin waves by a flow of charged particles was theoretically predicted in [68] under the conditions of Cherenkov synchronism—the drift velocity of charge carriers exceeds the phase velocity of spin waves. A necessary condition for the amplification of spin waves is the presence of a material with low attenuation of spin waves and high mobility of charge carriers. The first few attempts to amplify spin waves in YIG-semiconductor-based layered structures failed, because even in such perfect structures the conditions of Cherenkov synchronism could not be reached yet. The amplification of spin waves in magnetic SCs, such as HgCr_2Se_4 with a charge carrier mobility of $\sim 10^3$ cm²/(V·s), became possible due to the low phase velocity of $10^5\text{--}10^6$ cm/s of excited spin waves, which are

2–3 orders of magnitude slower than those in the YIG-layered structures [69–71]. Spin waves in HgCr_2Se_4 were excited by longitudinal and transverse pumping with microwave radiation at a frequency of 9.4 GHz and a power of 5 kW. Figure 5 shows a multiple decrease in the attenuation of spin waves obtained in an n- HgCr_2Se_4 single crystal when a pulsed electric field with a duration of 2 μs and frequency of 16 Hz was applied at $T = 77$ K.

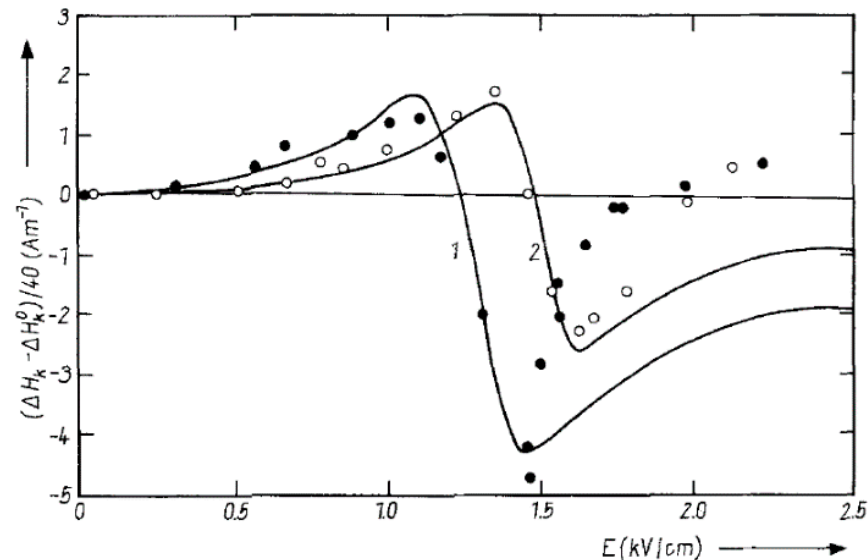


Figure 5. Spin-wave attenuation versus electric field for wavevector $k = 9.2 \times 10^5 \text{ cm}^{-1}$ (1), $k = 6.3 \times 10^5 \text{ cm}^{-1}$ (2) taken at temperatures below 80 K. Dots are experimental results; solid lines are modelling.

The effect is sensitive to the mutual orientation of the magnetic and electric fields. For example, it is absent if the electric field is perpendicular to the direction of propagation of the spin waves. An analysis of a large amount of experimental data made it possible to draw an important conclusion that the observed amplification of spin waves is due to the magnetoelectric mechanism inherent only in the magnetic SC, and theoretically predicted by E. Nagaev in [72].

Besides the drifting charge carriers, other technical solutions for the amplification of spin waves have also been considered. In particular, a spin-wave amplification based on the magnetoelectric effect was proposed to create spintronic logic devices in [73]. The device presents a layered structure consisting of a Si substrate, a magnetostrictive FM thin film, in which spin waves should propagate, and a piezoelectric layer with a metal gate (Figure 6). A voltage applied to the metal gate causes mutual deformation of the piezoelectric and FM layers. Due to the magnetostriction, the anisotropy axis in the FM layer can change its direction by up to 90 degrees. If the change in the gate voltage is synchronized with the oscillations of the spin waves, the amplification of the spin waves by several orders of magnitude become possible. It was assumed that such a structure can increase the attenuation length of spin waves tenfold, up to several hundred micrometers.

2.4. MR Structures Based on a p-n Junction in Magnetic SC

In relation to the comprehensive development of electronics, there is a huge number of applied problems associated with the creation of different magnetic devices (e.g., field indicators, sensors, memory elements, miniature electric motors, etc.) operating on the magnetoresistance (MR) effect. Magnetoresistance is a relative change in the electrical resistance of a medium under the influence of an external magnetic field. In the introduction, it was noted that bulk magnetic SCs can show CMR (depending on the composition it can reach up to 10⁶% [6]). However, large values of giant MR can also be obtained in artificially created nanostructures. In [74,75] an original method for obtaining MR was proposed in a structure based on a p-n junction in the $\text{La}_{1-x}\text{Ca}_x\text{MnO}_3$ and HgCr_2Se_4 magnetic SCs.

The method is based on changing the contact potential difference, electrical resistance and the thickness of charge carriers' depleted layers at the interface between p- and n-type SCs, possessing different Fermi levels, under an application of an external magnetic field. Two different ways for obtaining the p-n junction in single HgCr_2Se_4 crystals were used: 1—annealing of the single crystals in Hg vapor [58] and 2—replacing of Hg^{2+} ions with In^{3+} ions [59].

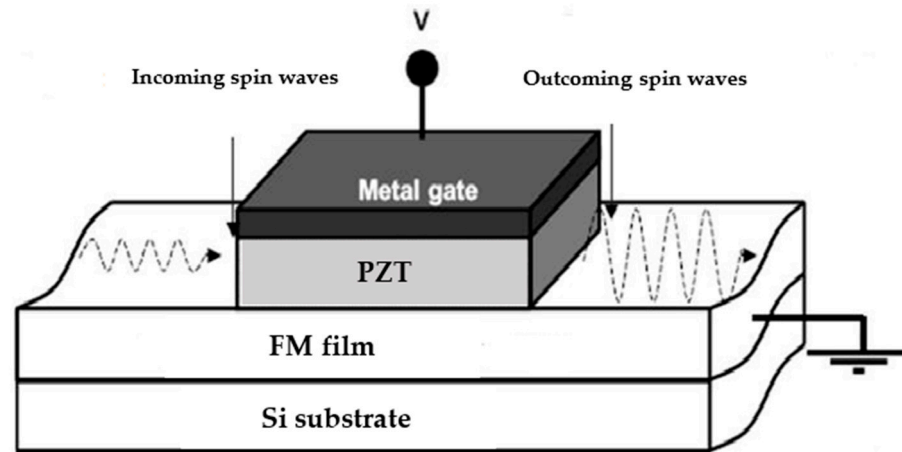


Figure 6. Magnetolectric element based on a layered structure: FM material (e.g., CoFe, NiFe) and a piezoelectric layer (e.g., PZT) [73].

Figure 7 shows the principal scheme of this method. There one can see an n-type magnetic SC layer with a thickness t_n and Fermi level E_F^n grown on the surface of a p-type magnetic SC with t_p and E_F^p . In the equilibrium state electrons diffuse from the n-region to the p-region while holes diffuse back into the n-region until the Fermi levels of the SCs are aligned. At the interface a space charge is formed and a contact potential difference occurs, which is determined by the difference between the Fermi levels $U_c = E_F^n - E_F^p$. The number of electrons that diffuse from the n- to the p-region on distance d can be estimated by the value $n_d = U_c \epsilon_0 / ed$, where ϵ_0 is the permittivity and e —the electron charge. The shaded parts in Figure 7 show d_n and d_p depleted layers of SC. Calculations showed that the common thicknesses of the depleted layer can reach ~ 1000 lattice constants. As a result, an intermediate layer with thickness $d_L = d_n + d_p$ becomes less conductive and the current flow through the p-n junction is diminished.

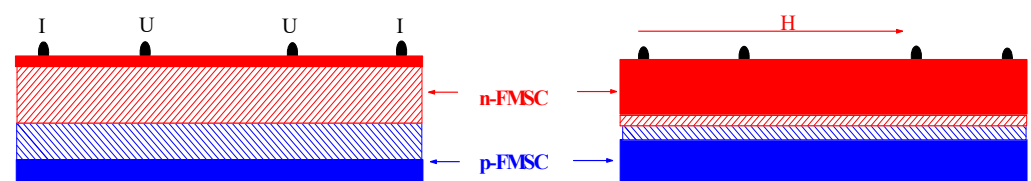


Figure 7. Schematic of structures based on a p-n junction in ferromagnetic SCs. The depleted layers are shaded. A four-fold contact scheme for measuring electrical and MR in magnetic field H is applied.

An exceptional feature of magnetic SC is the presence of a giant red shift of the absorption edge under the action of a magnetic field, and temperature-induced changes in the band structure [3,7]. At $T < T_C$, as a consequence of changes in the band structure, the transport of spin-polarized carriers through the p-n junction will change significantly. When a magnetic field is applied to the structure, both U_c and d_L decrease (Figure 7b), which leads to an increase in current flow through the p-n junction.

Figure 8 demonstrates a significant difference in the field dependences of the MR for the homogeneous p- and n-type HgCr_2Se_4 samples (in the inset) and for the structure based on a p-n junction in HgCr_2Se_4 under the same experimental conditions. At $T = 125$ K, in

the structure based on the p-n junction there is a ~50-fold increase in the MR compared to the data for p-HgCr₂Se₄.

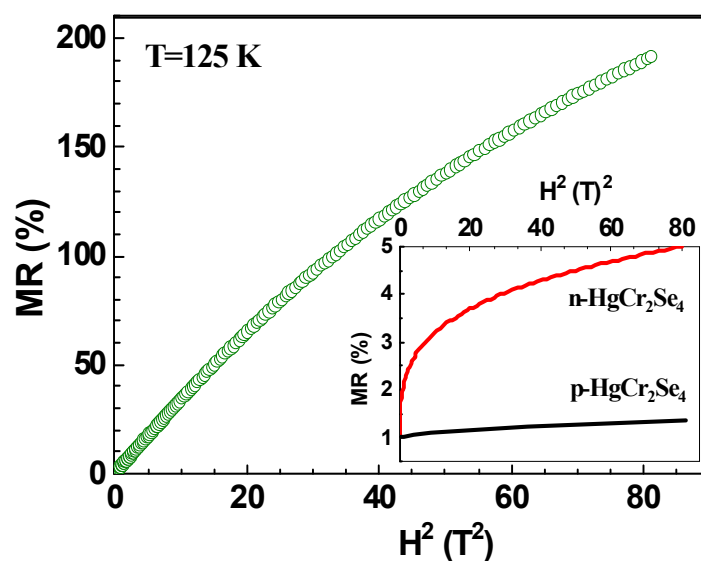


Figure 8. Field dependences of magnetoresistance MR for p-n structure of HgCr₂Se₄ at $T = 125 \text{ K} \approx T_C$. The inset shows the field dependences of the MR of the initial crystals of n-HgCr₂Se₄ and p-HgCr₂Se₄.

It was also assumed that such p-n junction structures can also be created by using other magnetic SCs, such as EuO, EuSe and CdCr₂Se₄. For example, a diode was created based on a p-n junction in thin-film manganites with CMR [76]. At room temperature, i.e., in the semiconducting regime, it was shown to exhibit asymmetric current–voltage (I–V). The observed asymmetry in the I–V characteristics disappeared at low temperatures where both the manganite layers are metallic. Therefore, using the polaronic semiconducting regime of doped manganites a thin-film p–n diode can be constructed [76].

2.5. Magnetic SC with Tunnel Injection of Spin-Polarized Electrons

Besides the CMR effect in bulk magnetic SCs, there are many other mechanisms for obtaining large values for MR. For example, magnetoresistance associated with the tunneling of spin-polarized electrons through the crystallite boundaries was observed in polycrystalline and nanocrystalline manganites [6–8,44–48]. The tunneling MR in manganites appears below the Curie temperature and grows exponentially as the temperature drops to 0 K in contrast to the CMR, which is maximum only near T_C . While CMR has an almost linear dependence on a magnetic field of up to 1 T, the tunneling MR in manganites is highly sensitive and saturates in low magnetic fields. It is obvious to assume that the combination of these two phenomena could extend the temperature range of existent MR effect in manganites. There are different methods for fabrication of magnetic nanostructures. Recently an important technology was developed for producing thin epitaxial films of magnetic SC with a variant structure, in which tunneling and colossal MR coexist and reach high values in a wide temperature range [77]. Unlike polycrystals with randomly distributed crystallites, these films are formed by nanosized structural domains with strictly defined angular boundaries, the set of which does not change over the film thickness. CMR in such nanostructured films is associated with a change in resistance under the action of a magnetic field inside highly conductive structural domains while tunneling MR is associated with a change in the concentration of spin-polarized electrons tunneling through weakly conductive boundaries of structural domains. It was established that in the La_{0.8}Ag_{0.1}MnO₃ films spin-polarization of electrons reached ~0.5 [78]. High values of the effects in manganite films nanostructured by the epitaxial in-plane variants, such as

positive TMR in low fields, negative TMR at low temperature in higher fields and CMR near room temperature, can be used in various technical applications.

In a large number of works it was shown that CMR in $A_{1-x}B_x\text{MnO}_3$ -doped manganites ($A = \text{La, Pr, Nd, Sm}$; $B = \text{Sr, Pr, Ca, Na, Ag, K, etc.}$) has a high-frequency response in the infrared region of the spectrum predominantly associated with the interaction of light with both localized and delocalized charge carriers [79–81]. It appears as a magnetotransmission effect (MT) which is defined as—a relative change in the intensity of light transmitted by a sample under the action of an external magnetic field. Magnetotransmission is determined by the volume of FM phase, type and level of doping, sample thickness, the mechanical stresses and the interface phenomena in thin films [30,78–82]. It was shown that because of the quasi-local character of the MT (different optical responses from conducting and non-conducting areas) that the MT measurements are a good tool for studying the phase separation process and magnetic and charge inhomogeneity in CMR manganites [81,82]. The authors of [83] demonstrated that the nanoscale phase-separated manganites can be treated as natural metamaterials and peculiarities in their optical properties and MT and MR spectra can be connected with localized collective volume plasmon resonances at the metal-insulator interface.

Later, a contactless method for separating the contributions of CMR and tunneling MR in manganite films with the variant structure was proposed in [78,84]. The technique is based on a comparative analysis of the temperature dependences of MR and magnetotransmission of natural (non-polarized) light in the IR spectral range. As an example, Figure 9 shows the temperature dependences of MR and MT for $\text{La}_{0.8}\text{Ag}_{0.1}\text{MnO}_3$ films with the variant structure. An important fact is the presence of both the low-temperature “butterfly-like” hysteresis of MR associated with the tunneling of spin-polarized electrons (Figure 9) and MO response in the form of tunneling MT effect. The results of the study of nanostructured manganite films with high MR and MO effects in a wide temperature range can be used for creating various opto-spintronic devices.

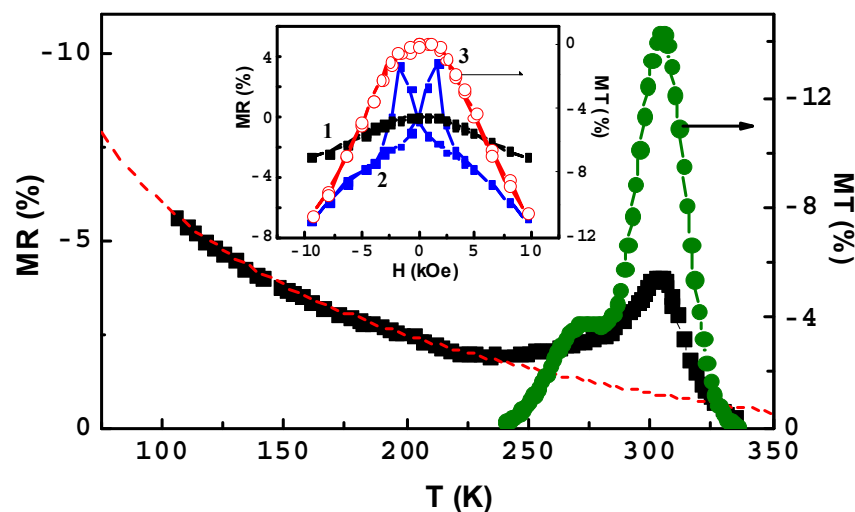


Figure 9. Temperature dependences of the magnetoresistance MR (left axis, square symbols) and the magnetotransmission MT (right axis, circle symbols,) at wavelength of $6 \mu\text{m}$ for $\text{La}_{0.8}\text{Ag}_{0.1}\text{MnO}_3$ films in the magnetic field of 8 kOe. The dashed red line is the result of the fitting by function $f = a + b/\sqrt{T}$. Inset: field dependences of MR (left axis) at $T = 295 \text{ K}$ (1) and $T = 80 \text{ K}$ (2) and MT (right axis) at $T = 295 \text{ K}$ (3) and wavelength of $6 \mu\text{m}$.

The presence of the large MT effect in lanthanum manganites is of great practical interest for the creation of a wide range of optoelectronic devices. Unfortunately, infrared MT in manganites only takes place near to T_C . The problem of expanding the temperature intervals of MR and MT can be solved in different ways, for example, by creating new functional materials based on thin-film heterostructures consisting of layers with

different T_C . Figure 10 demonstrates the temperature dependences of the MT and MR for the $\text{Sm}_{0.55}\text{Sr}_{0.45}\text{MnO}_3\text{--Nd}_{0.55}\text{Sr}_{0.45}\text{MnO}_3$ heterostructure [85]. An important result is the appearance of a contribution of an interface layer of intermediate composition in the optical and electrical properties of the heterostructure. It is worth noting that the magnitude of the MT and MR in the interface layer with thickness ~ 10 nm was comparable to the magnitude of the effects in single layer films.

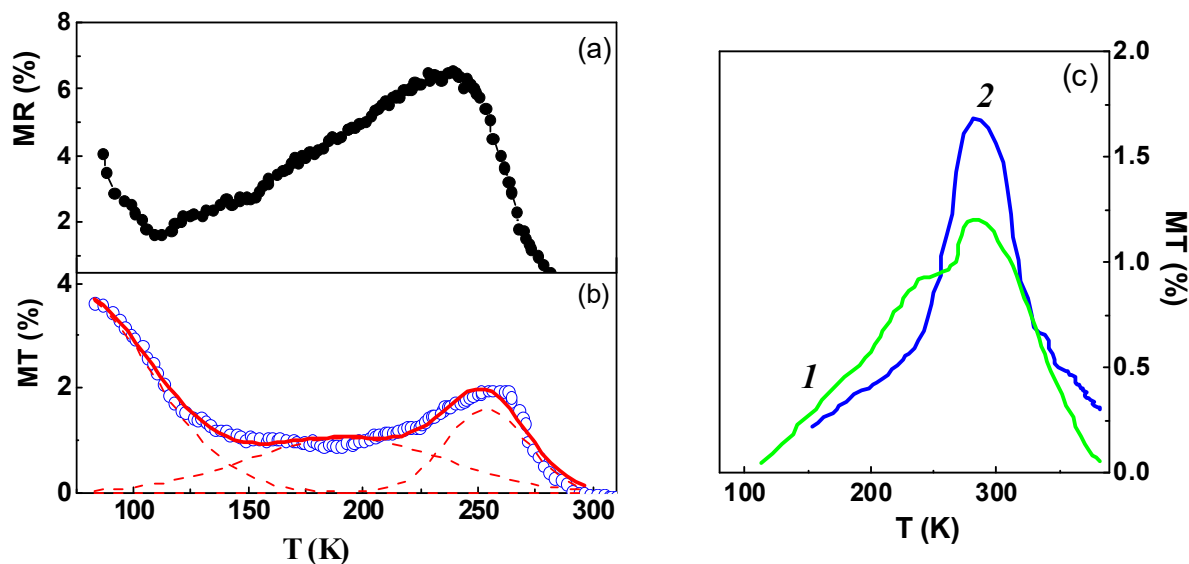


Figure 10. Temperature dependences of the absolute value of (a) the colossal MR and (b) magnetotransmission MT at wavelength of 3 μm for the $\text{Sm}_{0.55}\text{Sr}_{0.45}\text{MnO}_3\text{--Nd}_{0.55}\text{Sr}_{0.45}\text{MnO}_3$ thin-film heterostructure in the magnetic field of 8 kOe. The dashed lines are the Gaussian fitting for each thin-film layer and the interface, the solid red line is the result of the fitting; (c) temperature dependences of the absolute value of MT for the single-layer $\text{La}_{0.7}\text{Sr}_{0.3}\text{MnO}_3$ film (1) and thin-film $\text{CoFe}_2\text{O}_4/\text{La}_{0.7}\text{Sr}_{0.3}\text{MnO}_3$ heterostructure (2) at wavelength of 6 μm in the magnetic field of 8 kOe.

The processes of tunneling of spin-polarized electrons through an interface in heterostructures and its manifestation in magnetotransport and MO properties were also considered in $\text{La}_{2/3}\text{Ca}_{1/3}\text{MnO}_3/\text{La}_{2/3}\text{Sr}_{1/3}\text{MnO}_3$ and $\text{La}_{2/3}\text{Ca}_{1/3}\text{MnO}_3/\text{SrTiO}_3/\text{La}_{2/3}\text{Sr}_{1/3}\text{MnO}_3$ manganite thin-film heterostructures [86]. It was shown that the presence of a 2-nm-thick SrTiO_3 barrier layer does not affect the shape and position of the MT maximum in a magnetic field applied perpendicularly to the heterostructure surface. At the same time, the barrier leads to an increase in MR and to the extra contribution in MT from the lower layer due to the tunneling of spin-polarized current carriers through the barrier.

The presence of two or more layers with different magnetic permeabilities leads to biasing of a layer with a lower T_C and to gain the magnitude of control of magnetic fields. For example, in [46,87] the enhancement of the effects of MR and MT was demonstrated in $\text{La}_{0.7}\text{Sr}_{0.3}\text{MnO}_3/\text{ferrite}$ heterostructures (ferrite-spinel— CoFe_2O_4 , MnFe_2O_4 , $\text{Nd}_3\text{Fe}_5\text{O}_{12}$, $(\text{Nd}_{0.75}\text{La}_{0.25})_3\text{Fe}_5\text{O}_{12}$, etc.). The gain in the magnetic field obtained in these heterostructures was $\sim 40\%$ (Figure 10c). A tenfold gain in the magnitude of controlled magnetic fields was also obtained in the $(\text{La}_{0.25}\text{Pr}_{0.75})_{0.7}\text{Ca}_{0.3}\text{MnO}_3/\text{YBa}_2\text{Cu}_3\text{O}_{7-y}$ heterostructure due to the concentration (amplification) of the magnetic flux in a window (hole) in a high-temperature superconductor layer [88].

Therefore, new functional materials based on manganites with improved characteristics can be obtained in various ways. Based on the MO and MR effects described in this section, working layouts of various optoelectronic devices can be created. A brief description of some of them will be given below.

2.6. Spin Valve Structures

A spin valve is a device in which the current of spin-polarized carriers appears when an external magnetic field is applied. Often many such devices work as a diode or a spin switch. The scheme of a spin valve based on a magnetic SC thin-film structure is shown in Figure 11. The device operates on the basis of tunneling spin-polarized charge carriers from a ferromagnetic $\text{La}_{1-x}\text{Ag}_x\text{MnO}_3$ through a high-resistance barrier layer (an insulator or a high-resistance ferromagnetic or non-magnetic SC, for example, Ag_2O , NiFe_2O_4 , $\alpha\text{-Fe}_2\text{O}_3$) into a metal (e.g., NiFe film). The field dependence of the MR in Figure 11 demonstrates a sharp change ($\sim 17\%$) in the electrical resistance of the structure when a magnetic field as small as 50 Oe is applied at $T = 77\text{ K}$, i.e., fulfillment of the spin valve condition [89]. At room temperature the MR is about 3%.

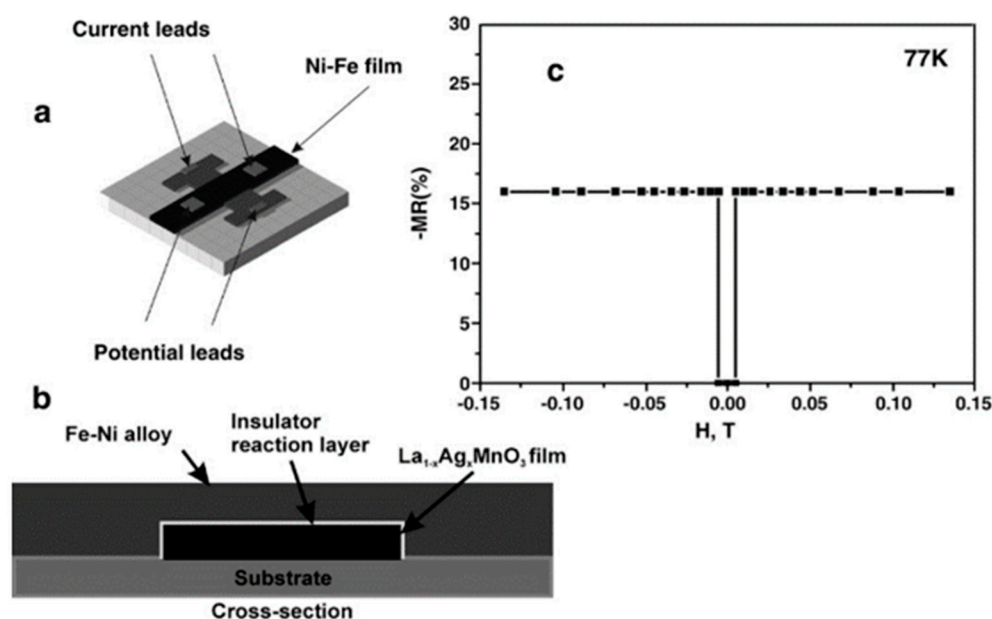


Figure 11. Schematic representation of the spin valve: (a) top view, (b) cross-sectional view, (c) field dependence of the magnetoresistance MR of the spin valve [89].

At present, new magnetoelectric materials such as multiferroics are being intensively studied. These functional materials suggest a different approach to spintronics, excluding the use of spin currents [90–92]. Since multiferroics are magnetoelectric materials, they can be used to convert magnetization into electrical voltage and vice versa. Particular attention is paid to magnetic SC films of BiFeO_3 , in which switching of antiferromagnetic domains under the action of an electric field has been found [90]. The external electric field causes the electric polarization to switch from one crystallographic direction to another, which leads to a switch in the direction of the sublattice magnetizations via the coupling of the electric and magnetic subsystems of the multiferroic. A model of a thin-film spin switch is schematically shown in Figure 12. The magnetic moment associated with the antiferromagnetic order of BiFeO_3 is small ($\sim 5\text{ Oe}$, a weak FM due to the canting of antiferromagnetic sublattices). However, it can be applied to switch the magnetization of a FM layer after the deposition of an additional FM layer. Such a spin switch is proposed to be used as an element of random-access magnetic memory, combining the speed of SC electronics with the non-volatility of magnetic memory. According to a press release from Fujitsu, they created a composite based on BiFeO_3 , which can increase the amount of stored information by 5 times compared to previous generations of FeRAM (ferroelectric random access memory) using PZT ceramic ($\text{Pb}(\text{Zr},\text{Ti})\text{O}_3$). The review of the physical properties of multiferroics and their potential for practical purposes, including spintronics, is given in [91] and references therein. For example, a display of modulators based on the Faraday effect in multiferroics was created [92].

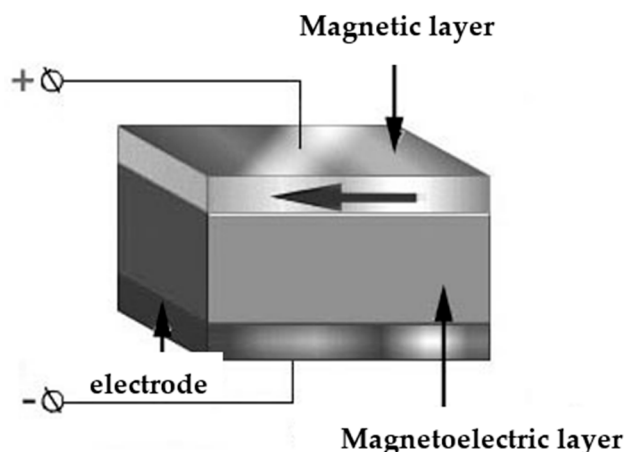


Figure 12. A schematic model of a spin switch.

2.7. Amplitude Modulation of Light

A modulator of EM radiation is a device with transparency controlled by an external influence. For example, it can demonstrate a periodic or non-periodic change in the intensity of visible or infrared radiation under the influence of a magnetic field [27–29,31,93]. Initially, an amplitude modulator working in the range from 1.5 to 11 μm was created based on the effect of MT of unpolarized light in a thin $\text{La}_{0.82}\text{Na}_{0.18}\text{MnO}_3$ film [31]. Such a modulator could operate in a narrow temperature range near room temperature (Figure 13).

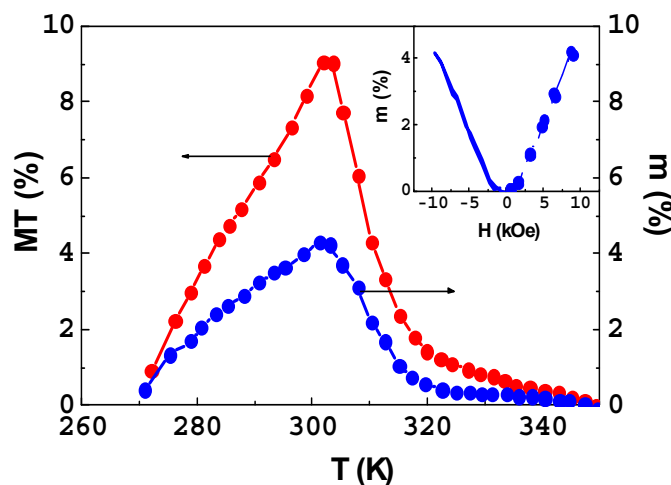


Figure 13. Temperature dependencies of the absolute value of magnetotransmission MT (left axis, red symbols) and modulation depth m (right axis, blue symbols) of a modulator based on $\text{La}_{0.82}\text{Na}_{0.18}\text{MnO}_3$ film in a magnetic field of 8 kOe and wavelength of 8.8 μm . The inset shows the field dependence of m at $T = 303$ K in a constant field (solid line) and in an alternating magnetic field (circles).

The inset shows the field dependence of the MT and modulation depth $m = (I_{max} - I_{min}) / (I_{max} + I_{min}) = (I_H - I_0) / (I_H + I_0)$, where I_{max} and I_{min} are the maximum and minimum intensity of the radiation transmitted through the MO element. The MT is an even effect and as a consequence the modulated light has a frequency equal to twice the frequency of an alternating magnetic field source. It was shown that in the $\text{La}_{0.7}\text{Ca}_{0.3}\text{MnO}_3$ film the modulation depth reaches $\sim 15\%$ ($\text{MT} \sim 30\%$) at a temperature close to 0°C and $\sim 5\%$ at $T = 310$ K and $H = 4$ kOe for $\text{La}_{0.65}\text{Ba}_{0.35}\text{MnO}_3$ films, while in the $\text{La}_{0.35}\text{Pr}_{0.35}\text{Ca}_{0.3}\text{MnO}_3$ film the value of $m \sim 25\%$ ($\text{MT} \sim 50\%$) at $T = 175$ K in $H = 8$ kOe [29–31,94,95]. The demand for thermostabilizing of the MO element significantly complicates the design and energy consumption of the device.

Figure 14 shows the principal scheme of a modulator of IR radiation based on the MT effect in manganites and the picture of the prototype of the IR modulator embedded with a thermal stabilization system. It can be seen that it is quite simple. An important feature of the modulator is the absence of polarizers, which are traditional elements for many MO devices: modulators, bandpass filters, etc.

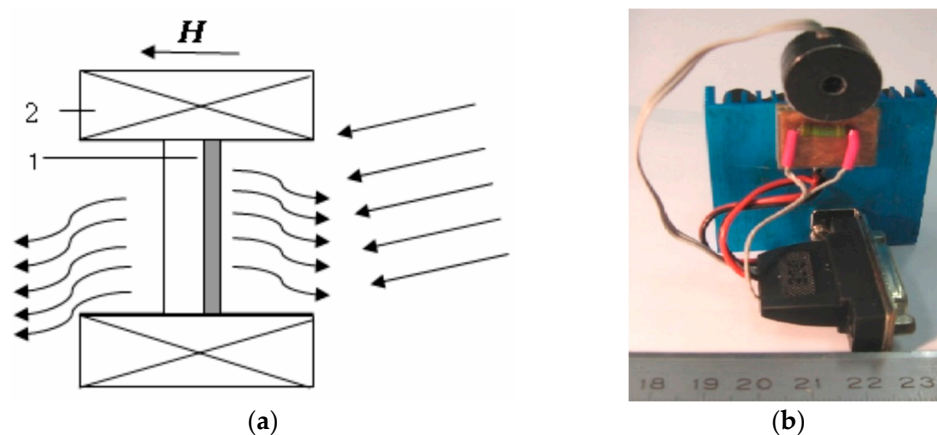


Figure 14. (a) The principal scheme of the modulator of IR radiation: 1—a MO element, 2—a source of permanent or alternating magnetic field H . Arrows indicate an incident light upon the sample, reflected and transmitted modulated radiation; (b) a prototype of the IR radiation modulator based on the effect of MT in a manganite film: black cylinder with center hole is a magnetic field source with MO element inside, blue plate with electrical contacts is a thermal stabilization system with controller.

The weak temperature dependence of the MR and MT in heterostructures consisting of layers with different T_C made it possible to create a modulator working without a thermal stabilization system in a wide temperature range [96]. The biasing of FM layers in the manganite/ferrite heterostructures can increase due to the magnitude of the controlled magnetic field in the IR modulator.

The aforementioned MO device is based on the effect of MT of light in lanthanum manganites with CMR. However, besides MT a giant magnetoreflection (MRf) of natural light can also be observed in manganites. As a result, being non-gyrotropic phenomena, MT and MRf lead to creating thin-film devices in which both the absorption and reflection of light can be changed simultaneously in a wide spectral range under the action of either temperature, magnetic, electric fields or in combination [97,98].

Implementation of the simultaneous controlling of the intensity of reflected and transmitted light is possible only using thin-film structures. The proposed approach has some advantages over the separate control of the reflected and transmitted light. It allows: (i) increasing the reliability of the optical signal processing; (ii) improving the noise stability of the optical system and (iii) extending the spectral and temperature range while saving on the size of a working optoelectronic device.

It should also be noted that manganite films exhibit noticeable MT and MRf of light in the fundamental absorption region in the vicinity of the Curie temperature and at low temperatures [81,95,99]. The obtained values of the effects in the visible spectral range are less than those observed in the infrared range, but they are several times greater than the linear MO effects. The physical mechanisms responsible for causing MRf and MT define the working characteristics of the proposed method of amplitude modulation of light. They are related to: (i) suppression of the magnetic moment fluctuations of the charge carriers in the vicinity of the magnetic phase transition and (ii) field-induced changes of tunneling (scattering) of spin-polarized charge carriers.

Therefore, this aforementioned approach of simultaneous controlling of the intensity of reflected and transmitted light in manganites was shown to be applicable in the wide visible and IR spectral ranges from 0.3 to 21 μm (4.1–0.06 eV), the temperature range from liquid helium temperatures to 360 K and in magnetic fields of a few kOe ($\sim 10^5$ A/m) (see Table 1

for examples). This simple scheme of light modulation is very promising because there is no need for using any light analyzers and polarizers in optical circuits. Another more important parameter is the speed of response in the proposed method of light modulation, which is limited by the technical characteristics of a magnetic flux source, detector, light source, etc. It was shown that MT in manganites in alternating fields has the same values as in the constant field at the frequencies up to $\omega = 1$ kHz (Figure 13) and the frequency limit range can attain a few GHz [31,93,96]. Recently it was also demonstrated that the speed of MO response of magnetic SCs can be increased up to 10^{15} Hz if short-pulsed lasers are used as a radiation source [98,100–102].

Table 1. The absolute values of magnetotransmission (MT) at wavelength $6 \mu\text{m}$ (0.2 eV) and colossal magnetoresistance (CMR), and the Curie temperature (T_C) for doped manganite films in magnetic field $H = 7.5$ kOe.

Film	MT, %	CMR, %	T_C , K
$\text{La}_{0.7}\text{Ca}_{0.3}\text{MnO}_3$	25	33	259
$(\text{La}_{0.75}\text{Pr}_{0.25})_{0.7}\text{Ca}_{0.3}\text{MnO}_3$	25	45	214
$(\text{La}_{0.5}\text{Pr}_{0.5})_{0.7}\text{Ca}_{0.3}\text{MnO}_3$	23	60	179
$(\text{La}_{0.25}\text{Pr}_{0.75})_{0.7}\text{Ca}_{0.3}\text{MnO}_3$	4	21	79
$\text{La}_{0.67}\text{Sr}_{0.33}\text{MnO}_3$	6	8	356
$\text{La}_{0.67}\text{Ba}_{0.33}\text{MnO}_3$	10	25	306
$\text{La}_{0.8}\text{Ag}_{0.1}\text{MnO}_{3+\delta}$	11	8	301
$\text{La}_{0.85}\text{Ag}_{0.15}\text{MnO}_3$	9	17	316
$\text{La}_{0.82}\text{K}_{0.18}\text{MnO}_{3+\delta}$	6	19	280

MO devices based on manganites can also operate with linearly polarized light in the visible region at $\lambda < 0.8 \mu\text{m}$ ($E = 1.55$ eV). For example, a large Faraday effect was found for thin films of Sr-doped manganites in the visible range [103]. Moreover, controlled transponders and matrices of modulators are currently being actively developed based on the Faraday effect in garnet-ferrites, the so-called spatial MO modulators (MOSLM—magneto-optical spatial light modulator). For example, the size of the real display-matrix of 20×20 elements is $100 \times 100 \times 5 \mu\text{m}^3$ [104–106].

2.8. Optical Branch of Straintronics: Strain-Magneto-optics

Recently, a new branch of spintronics, straintronics, has emerged, studying the effect of elastic distortions caused by external fields on the physical properties of various objects, including materials with a magnetic order, e.g., magnetic SCs [107]. Optical reflection and absorption in magnetics are sensitive to magnetic field and mechanical deformation. This sensitivity is exploited in many devices.

Though MO phenomena associated with magnetoelastic interactions in magnetic SCs are well known, the detailed study of the correlation between magnetostriction and magnetoabsorption of natural light in ferrite spinel (e.g., CoFe_2O_4) in the IR spectral range has only recently been completed [108,109]. It was shown that the strain-induced MO properties of CoFe_2O_4 manifest themselves as a correlation of the field dependences of magnetostriction, magnetoreflexion and magnetoabsorption (Figure 15).

These effects reach large values in the IR range ($\sim 5\%$ in $H \sim 3.5$ kOe at room temperature) and are ascribed to the sensitivity of the fundamental absorption edge and impurity absorption bands to the strain and distortions of the crystal lattice [110,111]. A close interplay between MO and magnetoelastic properties in ferrite spinel materials with anomalously strong magnetostriction indicates that such compounds should be considered a special class of optical materials, and in the corresponding field of magneto-optics can be classified as strain-magneto-optics [109]. Strain-magneto-optics is promising for creating new spintronic devices based on magnetic SCs, e.g., polarization-independent IR modulators.

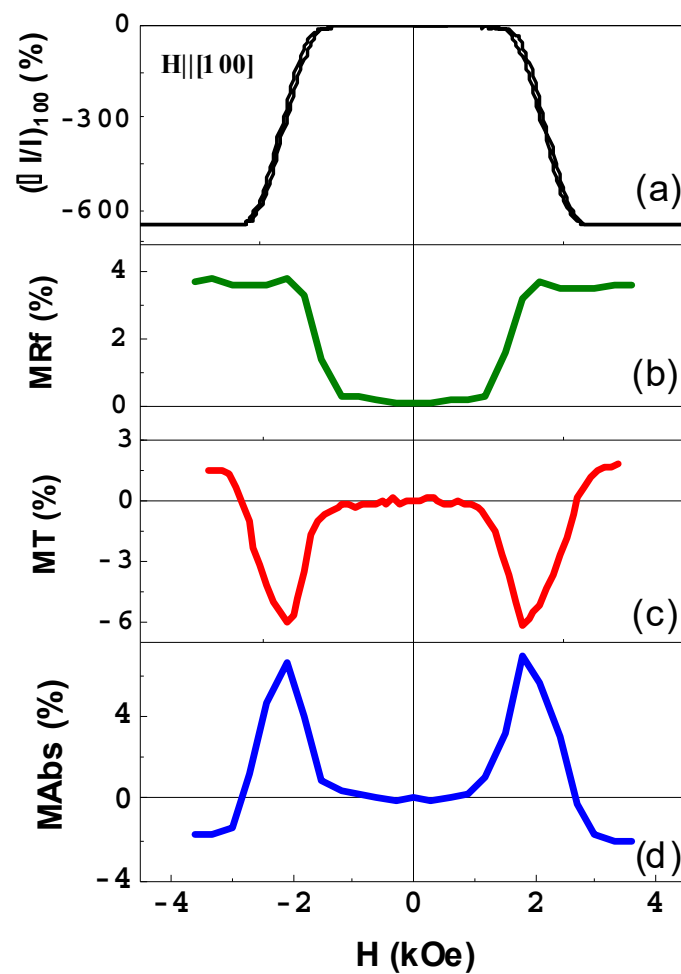


Figure 15. Magnetic field dependences of (a) linear magnetostriction $(\Delta l/l)_{100}$; (b) magnetoreflexion MRf; (c) magnetotransmission MT and (d) magnetoabsorption of light MAbs of the CoFe_2O_4 single crystal for orientation of magnetic field $H \parallel [100]$ at wavelength of $2.7 \mu\text{m}$ and $T = 295 \text{ K}$.

2.9. A “Magnetic Lens”—Manganite/HTSC Heterostructure

A new original method of reducing the driven magnetic fields in MO devices was presented in [88]. In Figure 16 a scheme is shown of so-called “magnetic lens” based on a thin-film manganite/HTSC heterostructure. The “magnetic lens” includes a layer of manganite $(\text{La}_{0.25}\text{Pr}_{0.75})_{0.7}\text{Ca}_{0.3}\text{MnO}_3$ grown on an insulator single crystal perovskite substrate with a $\text{YBa}_2\text{Cu}_3\text{O}_{7-y}$ layer on the top. The former has a 2 mm in diameter hole in the middle of the HTSC film. The effective Curie temperature of the manganite layer and, consequently, the temperature of the maximum MT in the manganite is chosen to be close to the critical temperature of the HTSC. The HTSC layer plays the crucial role of a magnetic flux concentrator or “magnetic lens”.

The field dependence of MT in the manganite/HTSC heterostructure demonstrates the same value of the effect as in $(\text{La}_{0.25}\text{Pr}_{0.75})_{0.7}\text{Ca}_{0.3}\text{MnO}_3$ single layer manganite film but in lower magnetic fields under the same conditions (Figure 16). The decrease in the magnetic field for the heterostructure is due to the expulsion of magnetic flux lines from the HTSC into the manganite in the region of the hole in the HTSC. Therefore, there is a concentration of the magnetic flux, i.e., field amplification, the effect of the “magnetic lens”. Therefore, the $(\text{La}_{0.25}\text{Pr}_{0.75})_{0.7}\text{Ca}_{0.3}\text{MnO}_3/\text{YBa}_2\text{Cu}_3\text{O}_{7-y}$ heterostructure with a window in the HTSC layer can be applied for the creation of contactless optoelectronic devices with lower operating magnetic fields.

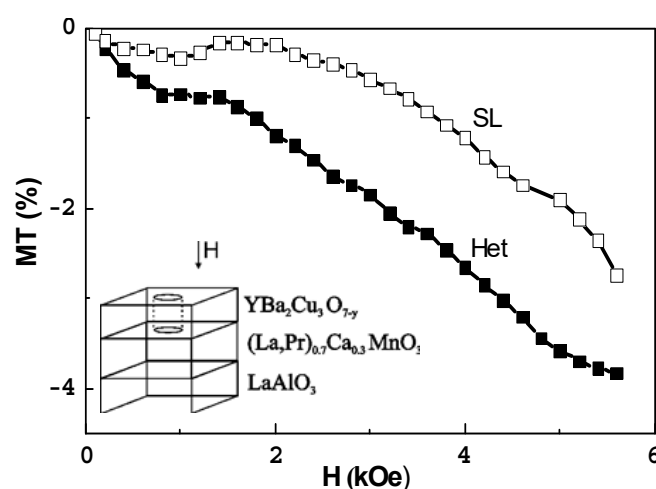


Figure 16. Field dependence of magnetotransmission MT at wavelength of 3.4 μm and $T = 67$ K for SL— $(\text{La}_{0.25}\text{Pr}_{0.75})_{0.7}\text{Ca}_{0.3}\text{MnO}_3$ single layer film; Het—heterostructure $(\text{La}_{0.25}\text{Pr}_{0.75})_{0.7}\text{Ca}_{0.3}\text{MnO}_3/\text{YBa}_2\text{Cu}_3\text{O}_{7-y}$. Inset: schematic representation of the prototype of magnetic lens based on the $(\text{La}_{0.25}\text{Pr}_{0.75})_{0.7}\text{Ca}_{0.3}\text{MnO}_3/\text{YBa}_2\text{Cu}_3\text{O}_{7-y}$ heterostructure. The arrow shows the direction of the external magnetic field H.

3. Nanocrystalline Magnetic Semiconductors—New Functional Materials for Spintronics

Nanocrystalline magnetic SCs are of interest both for fundamental problems of condensed matter physics and for practical applications, due to the appearance of new properties, when the particle size of a SC is reduced to the nanometer scale [112–114]. For the past decade the development of magnetic materials, particularly manganites and ferrites in nano-form, has undergone a fast evolutionary growth as strategic materials in spintronics and sensor applications [115–118]. At the same time, the concentration of defects in nanomaterials is much higher than in equilibrium single or polycrystals. This factor also significantly determines the properties of nanomaterials, transforming nanosized magnetic SCs into multifunctional materials. The features and the possibility of using nanosized ferromagnetic SCs as functional materials are well studied. Meanwhile, similar features are also manifested in nanosized antiferromagnetic SCs. For example, the presence of linear dichroism ($\sim 50\%$) allows for the use of antiferromagnetic semiconductor CuO as polarizers of infrared radiation [119]. Electron-field emission in CuO nanofibers is recommended for use in displays [120]. Irradiated nanocrystalline CuO oxides can accelerate reaction-catalytic effects in the production, for example, of alcohols. Moreover, the synthesis rate, for example, of copper phthalocyanine, can be controlled by a magnetic field at room temperature [121,122]. Nanocrystalline CuO is used in electronics as a buffer layer in complex thin-film electronic nanodevices [63]. Moreover, it can enhance an electrochemical activity, which is promising for use as electrodes in lithium current sources [123] and as an analyzer of carbon dioxide concentration [124]. However, there are problems in obtaining high-quality optically transparent SC nanomaterials of various types (powder, ceramic, fiber, and film).

3.1. High-Density Magneto-Optical Nanoceramics

For creating ceramics from a nanocrystalline material, important conditions are the preservation of the composition and size of compacted particles. Since magnetic SCs are multicomponent compounds, the production of high-density nanoceramics is rather complicated. To create nanoceramics, dynamic and static loading methods for obtaining high-density bulk nanomaterials are used. Static loading refers to the method of severe plastic deformation—shearing under pressure of at least 8 GPa. In this method, the number of distortions is determined not only by the applied high static pressure, but also by the angle of rotation of the anvils. For the creation of nanoceramics based on magnetic SCs,

special high-pressure chambers were developed [125,126]. For example, using the static deformation method, LaMnO_{3+y} nanoceramics with a density of 99% and grain sizes close to those of a nanopowder can be obtained [127]. It was also found that at high degrees of deformation and small crystallite sizes, the magnitude of micro-deformations in nanoceramics decreases, which may be due to more efficient relaxation of lattice stresses by grain boundary sliding with a decrease in crystallite size.

Dynamic loading refers to the method of explosive action on a low-density (polycrystalline powder compact) coarse-grained material made of a magnetic SC by spherically converging shock waves, as well as pressing axially-symmetric workpieces under the action of an explosion [67,128]. When exposed to spherically converging shock waves, the material is placed in a spherical steel hermetic case, in which, at the moment of a spherical explosion, the material is simultaneously compressed in all ways and a nanostructure is formed. During explosive pressing of axially-symmetric workpieces, the material is placed in a steel cylinder, in which, at the moment of explosion, the detonation wave propagates along the generatrix axis. The integrity of specially designed metal covers is not violated, which protects the resulting nanoceramics from contamination. The created nanoceramics show high temperature- and time-stability. As a result, the advantage of the developed methods is the ease of implementation, the combination of the creation of a nanostructure and material compaction in a single process, the production of high-density (~99%) stable nanosized materials and the absence of external contaminants. The results can be used for obtaining nanoceramics from a wide range of materials. Some fragments of real SC nanoceramics prepared by various methods are shown in Figure 17. It can be seen that the described methods allow obtaining dense nanomaterials of quite large geometrical sizes.

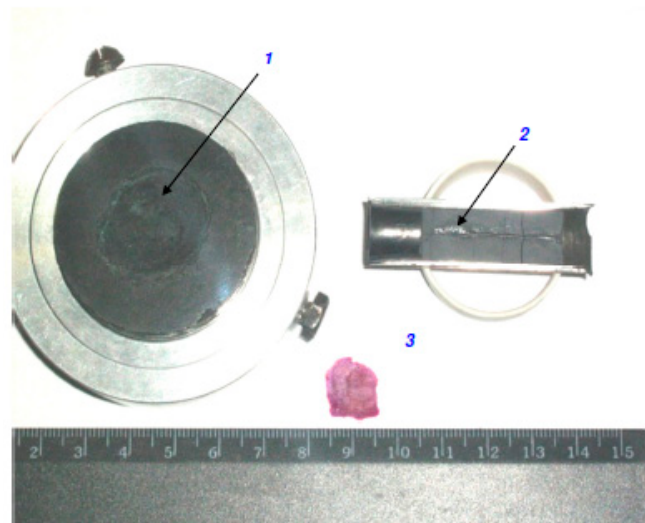


Figure 17. High-density nanoceramics obtained (1) by the method of spherically converging shock waves (CuO); (2) by the method of cylindrical explosive loading (LaMnO_{3+y}); (3) by the method of static pressure with shear ($\text{Y}_3\text{Fe}_5\text{O}_{12}$).

The promising technological process for creating high-quality dense nanoceramics of magnetic SC based on binary and even ternary compounds, such as CuO , Cu_2O , Mn_3O_4 , ZrO_2 , ZnSe , LaMnO_{3+y} , FeBO_3 , $\text{Y}_3\text{Fe}_5\text{O}_{12}$, etc., has been developed at the Institute of Metal Physics UB of RAS, Russia. The average particle size varies from 10 to 100 nm. The crystal structure, microstructure, imperfection, microhardness, magnetic, optical and other properties of the obtained nanomaterials have been studied in [129–134]. It has been established that the specific defectiveness of nanoceramics of magnetic oxides is ascribed to either the high concentration of oxygen vacancies, their agglomerates concentrated at the boundaries of crystallites or both, which determines (along with the nanostructure) the nonequilibrium nature of nanoceramics and the features of their mechano-chemical

properties. For example, anomalies in the magnetic properties, a decrease of the forbidden band gap and a negative thermal expansion for nanoceramics were found.

In the creation of new functional nanomaterials, the production of transparent nanoceramics is very important. The aforementioned techniques made it possible to create transparent nanoceramics with a high Faraday effect, i.e., the rotation of the plane of polarization of linearly polarized light passing through nanoceramics under the influence of an external magnetic field.

3.2. Nanocrystalline $Y_3Fe_5O_{12}$ as a New Magneto-Optical Material

An optically transparent high-density (density 99.6%) $Y_3Fe_5O_{12}$ (YIG) nanoceramic (Figure 17) was obtained by means of a sheared static pressure of ~ 50 GPa. The authors of [135,136] showed that the absorption coefficient of nanoceramic $Y_3Fe_5O_{12}$ in the transparency window is below 50 cm^{-1} . It is mainly due to light scattering by crystallites and varies slightly with reduction of grain size. As the degree of deformation of YIG nanoceramics increases, the concentration of defects changes and the magnitude of micro-deformations decreases. However, these factors have only little effect on the absorption coefficient in the transparency window. Figure 18 shows that the value of the Faraday rotation for nanoceramics of YIG is only 1.5 times less than that for the YIG single crystals and exceeds 50 deg/cm . It is important that as the grain size decreases, the Faraday effect increases, and then, starting from a grain size of 21 nm, the effect decreases again. The observed increase of the Faraday effect in nanosized magnetic SCs was theoretically explained in [137]. It was shown that electric dipole transitions in clusters of mixed valences of 3d ions in nanosized magnetic materials with the structure of perovskite and garnet can lead to a resonant enhancement of the MO activity in the limited area of deformations. Finally, transparent high-density nanoceramics based on magnetic SCs can be widely used for creation of various high-frequency and microwave sensors and shields and MO devices, in particular, IR radiation modulators, displays, etc.

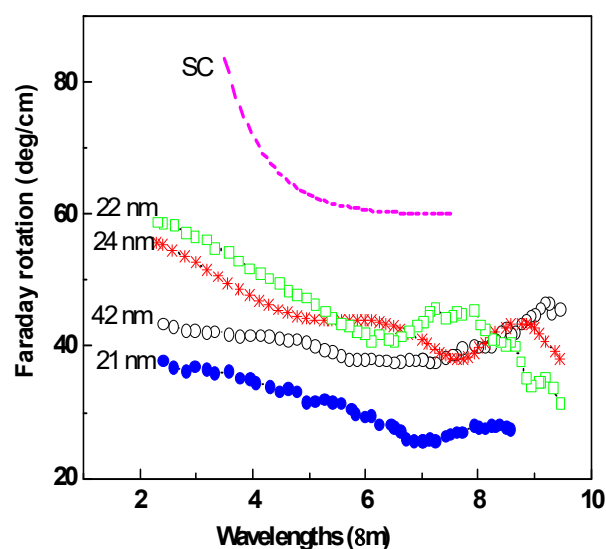


Figure 18. Specific Faraday rotation of nanostructured YIG samples with different crystallite sizes, SC–YIG single crystal.

3.3. Nanocrystalline CuO as a Material for Selective Solar Energy Absorbers

In relation to the problem of energy saving, great interest has arisen in alternative green energy sources, in particular, in selective absorbers of EM radiation and thermal converters of solar energy with coatings based on selective absorbers [138]. A selective solar energy absorber must meet certain requirements. For example, it should have a large absorption coefficient and a low reflection coefficient in the spectral range of solar radiation—in the energy range $E > 0.5$ eV. On the other hand, the absorber should have low electromagnetic

energy emission or high reflectance at $E < 0.5$ eV. In other words, a selective absorber must absorb the energy of the radiation source as efficiently as possible but minimally re-emit it back into the atmosphere in the IR region of the spectrum. It was shown that copper oxides [139–141] can be used as selective absorbers in solar energy collectors with working temperatures up to $T \sim 500$ °C. However, these materials do not meet the above conditions well, since they have a large forbidden gap. The authors of [142,143] demonstrated that this problem can be solved by changing the absorption spectrum of CuO practically without changing the refractive index when the copper oxide is transferred to the nanocrystalline state. Figure 19 shows the optical density (absorption) spectra for CuO single-crystal, nanopowder and nanoceramic, respectively.

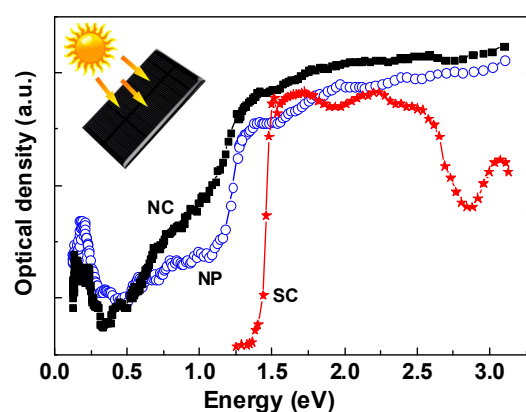


Figure 19. Optical density spectra of CuO samples at $T = 295$ K: SC—single crystal, NP—nanopowder, NC—nanoceramics.

The reasons for such strong changes in the spectra of CuO nanopowders and nanoceramics in the region of the main fundamental absorption edge were associated with a high level of defects and micro-deformations as well as with the behavior of strongly correlated materials in the nanocrystalline state. In CuO nanoceramics the observed energy changes that result in a significant decrease in the effective high-energy edge of the transparency window from 1.5 to 0.5 eV are the most pronounced [112,113].

It is necessary to note that there are many other directions in the development of technologies for obtaining nanoceramics and nanocomposites based on magnetic SCs and their possible applications in spintronics, nanophotonics, biology and medicine [144–148].

4. THz Magneto-optics in Magnetic Semiconductors

Today, the field of ultrafast magneto-optics is an important link between spintronics and ultrafast magnetism, which is necessary for understanding and controlling the processes of relaxation in the electronic, spin and lattice subsystems of a magnetic. The development of spintronics requires new materials with ultrafast spin transport at terahertz (THz) frequencies. Yet being underestimated, magnetic SCs can be one of the promising materials [149,150]. For example, chromium spinels have high charge carrier mobility, large infrared MO effects, high spin polarization level and numerous applied applications [151]. Recently the effects of magnetic linear birefringence and dichroism were observed in spinel crystals of $\text{Hg}_{0.92}\text{Cd}_{0.02}\text{Cr}_2\text{Se}_4$ in the frequency range 0.5–2.5 THz at temperatures below the magnetic ordering (Figure 20a) [152]. The maximal rotation of the light polarization plane induced by 1 kOe magnetic field reached about 4.3 rad/cm and was associated with a high-frequency response to the DC anisotropic MR in spinel. A large effect of magnetic field and temperature on the optical transmissivity of magnetic SCs in the proximity of a magnetic phase transition, is one of the manifestations of the spin-charge correlations. Employing a time-resolved pump-and-probe technique, the authors of [153] enabled determining of the lifetime of the electrons in the excited state of optical transitions. In the temperature range from 7 to 80 K, below T_C , it varied from 3 to 6 ps (Figure 20b). There was

also shown that the observed dependencies of the absorption spectrum and the lifetime of the electrons on the magnetic field and temperature qualitatively agree with the behavior expected for a weakly bound exciton coupled to the magnetic order.

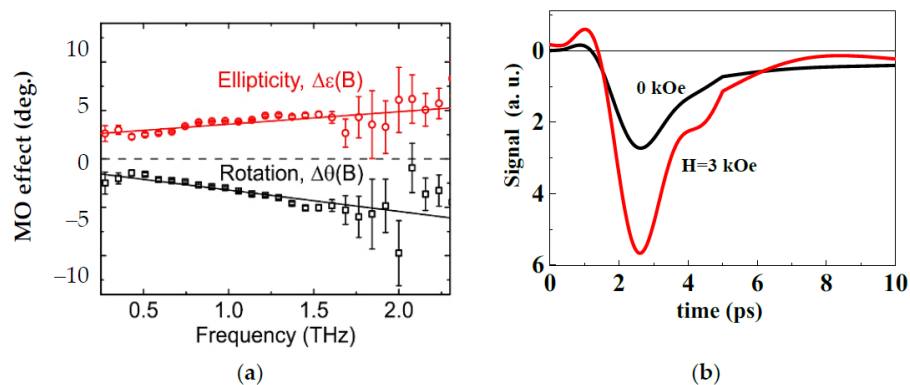


Figure 20. (a) Spectra of the magnetization-induced rotation and ellipticity of the transmitted THz radiation for $\text{Hg}_{0.92}\text{Cd}_{0.02}\text{Cr}_2\text{Se}_4$ single crystal at $T = 40$ K and 1 kOe applied field. The solid lines are linear fits used for guiding the eye [152]. (b) The temporal profile of the absorption of light in HgCr_2Se_4 single crystal at energy 0.23 eV (5.4 μm) and $T = 10$ K with and without an external magnetic field.

The femtosecond laser-pulse-induced oscillations of the magneto-optical Faraday rotation were considered in the FM semiconductor CdCr_2Se_4 . Two different mechanisms of photoinduced spin dynamics were assigned to the laser-induced heating and optical excitation of coherent spin oscillations having $\sim\text{ns}$ and $\sim\text{ps}$ relaxation processes, respectively [154]. Therefore, chromium spinel can be applied for studying various ultrafast phenomena in the wide spectral range from visible to THz frequencies. Detection of spin dynamics in magnetic SCs at times in the order of 10^{-12} – 10^{-15} s can significantly expand the functionality of IR and THz optoelectronic devices [100–102].

5. Conclusions

This review focuses on some advances towards the spintronic applications of magnetic semiconductors in the past two to three decades, during which experimental progress has been extraordinary. From the various aspects of spintronics, it presents ones devoted to the creation of new functional materials based on magnetic semiconductors and demonstrates the physical principles for solving some technical problems for creating various optoelectronic devices. Much attention is paid to the features of the physical properties of thin-film structures based on magnetic semiconductors. The possibility of practical use of such structures for creating the maser, p-n junctions with CMR, spin valves, magnetic lens and IR radiation modulators is demonstrated. Particular attention is paid to the methods of obtaining high-density transparent semiconducting nanoceramics. It is presented that nanoceramics can also be used as the solar energy absorber, IR radiation modulators, etc. It is also shown that THz magneto-optical phenomena and ultrafast spin dynamics in magnetic semiconductors are beneficial to the intensively developing fields of spintronics—ultrafast magneto-optics and magnetophotonics—and provide insight into the fundamental process of exchange between electron, phonon, and magnon subsystems in magnetics.

Nowadays, functional materials based on magnetic semiconductors are widely used for extending or modifying properties of many spintronic devices. Therefore, the authors are not able to give a full bibliography on magnetic semiconductors as spintronics materials in this review. Moreover, there are plenty of reviews that can give general readers more specific information. Since the authors believe that all the exciting effects in magnetic semiconductors will sooner or later find their application in spintronics, no comparative analysis of various technical solutions was also conducted.

Author Contributions: Conceptualization and writing—original draft preparation, Y.S.; writing—review and editing, supervision, project administration, A.T. All authors have read and agreed to the published version of the manuscript.

Funding: This research was supported by the program of the Ministry of Science and Education of Russia “SPIN” No. 122021000036-3, and “Brain Pool” program through the NRF funded by the MSIT of South Korea No. 2021H1D3A2A01096552.

Institutional Review Board Statement: Not applicable.

Informed Consent Statement: Not applicable.

Data Availability Statement: Not applicable.

Acknowledgments: The authors are grateful to Vivek Kumar Gaur for useful comments.

Conflicts of Interest: The authors declare no conflict of interest.

References

1. Methfessel, S.; Mattis, D.C. *Magnetic Semiconductors*; Wijn, H.P.J., Ed.; Springer: Berlin/Heidelberg, Germany; New York, NY, USA, 1968; pp. 389–562. [\[CrossRef\]](#)
2. Seeger, K. *Semiconductor Physics*; Springer Science & Business Media: Berlin/Heidelberg, Germany, 2013.
3. Nagaev, E.L. *Physics of Magnetic Semiconductor*; Mir Publishers: Moscow, Russia, 1983; p. 388.
4. Grundmann, M. *Physics of Semiconductors*; Springer: Berlin/Heidelberg, Germany, 2010; pp. 401–472.
5. Belov, K.P.; Tretyakov, Y.D.; Gordeev, I.V.; Koroleva, L.I.; Kesler, Y.A. *Magnetic Semiconductors—Chalcogenide Spinels*; Moscow State University: Moscow, Russia, 1981.
6. Nagaev, E.L. *Colossal Magnetoresistance and Phase Separation in Magnetic Semiconductors*; Imperial College Press: London, UK, 2002; p. 1.
7. Koroleva, L.I. *Magnetic Semiconductors*; Moscow State University: Moscow, Russia, 2003.
8. Barner, K. *New Trends in the Characterization of CMR-Manganites and Related Materials*; Research Signpost: Gottingen, Germany, 2005; p. 1.
9. Dionne, G.F. *Magnetic Oxides*; Springer: New York, NY, USA, 2009; p. 15.
10. Zvezdin, A.K.; Kotov, V.A. *Modern Magneto-optics and Magneto-optical Materials*; CRC Press: Boca Raton, FL, USA, 1997.
11. Telegin, A.V.; Sukhorukov, Y.P.; Bessonov, V.D.; Naumov, S.V. The Faraday effect in CoFe₂O₄ spinel ferrite in the IR range. *Tech. Phys. Lett.* **2019**, *45*, 601–604. [\[CrossRef\]](#)
12. Kimel, A.; Zvezdin, A.; Sharma, S.; Shallcross, S.; De Sousa, N.; Garcia-Martin, A.; Vavassori, P. The 2022 magneto-optics roadmap. *J. Phys. D Appl. Phys.* **2022**, *55*, 463003. [\[CrossRef\]](#)
13. Fumagalli, P.; Schoenes, J. *Magneto-Optics*; De Gruyter: Berlin, Germany, 2021. [\[CrossRef\]](#)
14. Telegin, A.V.; Sukhorukov, Y.P.; Loshkareva, N.N.; Mostovshchikova, E.V.; Bebenin, N.G.; Gan’shina, E.A.; Granovsky, A.B. Giant magnetotransmission and magnetoreflexion in ferromagnetic materials. *JMMM* **2015**, *383*, 104–109. [\[CrossRef\]](#)
15. Morgunov, R.B.; Dmitriev, A.I. Spin dynamics in magnetic semiconductor nanostructures. *Phys. Solid State* **2009**, *51*, 1985. [\[CrossRef\]](#)
16. Fetisov, Y.K.; Sigov, A.S. Spintronics: Physical foundations and devices. *Radioelektron. Nanosistemy Inf. Tehmol. RENSIT* **2018**, *10*, 343–356. [\[CrossRef\]](#)
17. Sato, K.; Katayama-Yoshida, H. Design of colossal solubility of magnetic impurities for semiconductor spintronics by the Co-doping method. *Jpn. J. Appl. Phys.* **2007**, *46*, L1120. [\[CrossRef\]](#)
18. Volkov, N.V. Spintronics: Manganite-based magnetic tunnel structures. *Phys. Uspekhi* **2012**, *55*, 250. [\[CrossRef\]](#)
19. Ivanov, V.A. Diluted magnetic semiconductors and spintronics. *Bull. Russ. Acad. Sci. Phys.* **2007**, *71*, 1610–1612. [\[CrossRef\]](#)
20. Yamada, Y.; Ueno, K.; Fukumura, T.; Yuan, H.T.; Shimotani, H.; Iwasa, Y.; Kawasaki, M. Electrically induced ferromagnetism at room temperature in cobalt-doped titanium dioxide. *Science* **2011**, *332*, 1065–1067. [\[CrossRef\]](#)
21. Rizal, C.; Shimizu, H.; Mejia-Salazar, J.R. Magneto-Optics effects: New trends and future prospects for technological developments. *Magnetochemistry* **2022**, *8*, 94. [\[CrossRef\]](#)
22. Awschalom, D.D.; Flatté, M.E. Challenges for semiconductor spintronics. *Nat. Phys.* **2007**, *3*, 153–159. [\[CrossRef\]](#)
23. Akinaga, H.; Ohno, H. Semiconductor spintronics. *IEEE Trans. Nanotechnol.* **2002**, *1*, 19–31. [\[CrossRef\]](#)
24. Hirohata, A.; Sukegawa, H.; Yanagihara, H.; Žutić, I.; Seki, T.; Mizukami, S.; Swaminathan, R. Roadmap for emerging materials for spintronic device applications. *IEEE Trans. Magn.* **2015**, *51*, 1–11. [\[CrossRef\]](#)
25. Bibes, M.; Barthelemy, A. Oxide spintronics. *IEEE Trans. Electron Devices* **2007**, *54*, 1003–1023. [\[CrossRef\]](#)
26. Gschneidner, K.A.; Pecharsky, V.K.; Pecharsky, A.O. Recent developments in magnetocaloric materials. *Rep. Prog. Phys.* **2005**, *68*, 1479. [\[CrossRef\]](#)
27. Loshkareva, N.N.; Sukhorukov, Y.P.; Gizhevskii, B.A.; Samokhvalov, A.A. Modulator of IR emission on magnetic semiconductors. *Pisma V Zhurnal Tekhnicheskoi Fiz.* **1989**, *15*, 83–86. (In Russian)

28. Loshkareva, N.N.; Sukhorukov, Y.P.; Samokhvalov, A.A.; Shuvalov, V.A.; Kartashev, E.V.; Chebotaev, N.M.; Naumov, S.V.; Aminov, T.G. Magnet-controlled band IR filter. *Pisma V Zhurnal Tekhnicheskoi Fiz.* **1992**, *18*, 10–13. (In Russian)
29. Sukhorukov, Y.P.; Loshkareva, N.N.; Samokhvalov, A.A.; Tugushev, S.N. Magneto-optic infrared modulator in the Voigt geometry. *Tech. Phys. Lett.* **1996**, *22*, 43–45.
30. Sukhorukov, Y.P.; Loshkareva, N.N.; Gan'shina, E.A.; Kaul, A.R.; Gorbenko, O.Y.; Fatieva, K.A. Giant change in the optical absorption of an $\text{La}_{0.35}\text{Pr}_{0.35}\text{Ca}_{0.3}\text{MnO}_3$ film near a metal-insulator transition and its possible application. *Tech. Phys. Lett.* **1999**, *25*, 551–554. [[CrossRef](#)]
31. Sukhorukov, Y.P.; Loshkareva, N.N.; Telegin, A.V.; Mostovshchikova, E.V.; Kuznetsov, V.L.; Kaul, A.R.; Vinogradov, A.N. IR radiation modulator based on the effect of magnetotransmission in lanthanum manganite operating near room temperature. *Tech. Phys. Lett.* **2003**, *29*, 904–906. [[CrossRef](#)]
32. Goyal, A.; Rajeswari, M.; Shreekala, R.; Lofland, S.E.; Bhagat, S.M.; Boettcher, T.; Kwon, C.; Ramesh, R.; Venkatesan, T. Material characteristics of perovskite manganese oxide thin films for bolometric applications. *Appl. Phys. Lett.* **1997**, *71*, 2535–2537. [[CrossRef](#)]
33. Heiras, J.; Pichardo, E.; Mahmood, A.; López, T.; Pérez-Salas, R.; Siqueiros, J.M.; Blanco, O.; Castellanos, M. Thermochromism in (Ba,Sr)-Mn oxides. *J. Phys. Chem. Solids* **2002**, *63*, 591–595. [[CrossRef](#)]
34. Sinitsyn, V.V.; Burmistrov, I.N.; Abrosimova, G.E.; Klinkova, L.A.; Bredikhin, S.I. Phase transitions and ionic conductivity of $\text{BaBi}_x\text{O}_{1.5x+1}$ ($x \geq 5$) oxides. *Ionics* **2006**, *12*, 69–71. [[CrossRef](#)]
35. Burmistrov, I.N.; Droshshin, O.A.; Istomin, S.Y.; Sinitsyn, V.V.; Antipov, E.V.; Bredikhin, S.I. $\text{Sr}_{0.75}\text{Y}_{0.25}\text{Co}_{0.5}\text{Mn}_{0.5}\text{O}_{3-y}$ perovskite cathode for solid oxide fuel cells. *J. Electrochem. Soc.* **2009**, *156*, 1212. [[CrossRef](#)]
36. Martinez-Boubeta, C.; Simeonidis, K.; Oró, J.; Makridis, A.; Serantes, D.; Balcells, L. Finding the limits of magnetic hyperthermia on core-shell nanoparticles fabricated by physical vapor methods. *Magnetochemistry* **2021**, *7*, 49. [[CrossRef](#)]
37. Moroz, P.; Jones, S.K.; Gray, B.N. Magnetically mediated hyperthermia: Current status and future directions. *Int. J. Hyperth.* **2002**, *18*, 267. [[CrossRef](#)]
38. Kuznetsov, A.A.; Shlyakhtin, O.A.; Brusentsov, N.A.; Kuznetsov, O.A. Smart mediators for self-controlled inductive heating. *Eur. Cells Mater.* **2002**, *3*, 75–77.
39. Pollert, E.; Knižek, K.; Maryško, M.; Kašpar, P.; Vasseur, S.; Duguet, E. New Tc-tuned magnetic nanoparticles for self-controlled hyperthermia. *JMMM* **2007**, *316*, 122–125. [[CrossRef](#)]
40. Melnikov, O.V.; Gorbenko, O.Y.; Markelova, M.N.; Kaul, A.R.; Atsarkin, V.A.; Demidov, V.V.; Soto, C.; Roy, E.J.; Odintsov, B.M. Ag-doped manganite nanoparticles: New materials for temperature-controlled medical hyperthermia. *J. Biomed. Mater. Res.* **2009**, *91A*, 1048–1055. [[CrossRef](#)]
41. Kessler, J. *Polarized Electrons*; Springer Science & Business Media: Berlin/Heidelberg, Germany, 2013; p. 299.
42. Gregg, J.F.; Petej, I.; Jouguelet, E.; Dennis, C. Spin electronics—A review. *J. Phys. D Appl. Phys.* **2002**, *35*, R121. [[CrossRef](#)]
43. Parkin, S.; Jiang, X.; Kaiser, C.; Panchula, A.; Roche, K.; Samant, M. Magnetically engineered spintronic sensors and memory. *Proc. IEEE* **2003**, *91*, 661–680. [[CrossRef](#)]
44. Borukhovich, A.S. Quantum tunneling in multilayers and heterostructures with ferromagnetic semiconductors. *Phys. Uspekhi* **1999**, *42*, 653. [[CrossRef](#)]
45. Zutic, I.; Fabian, J.; Das Sarma, S. Spintronics: Fundamentals and applications. *Rev. Mod. Phys.* **2004**, *76*, 323. [[CrossRef](#)]
46. Ziese, M. Extrinsic magnetotransport phenomena in ferromagnetic oxides. *Rep. Prog. Phys.* **2002**, *65*, 143. [[CrossRef](#)]
47. Dorr, K. Ferromagnetic manganites: Spin-polarized conduction versus competing interactions. *J. Appl. Phys.* **2006**, *39*, R125. [[CrossRef](#)]
48. Haghiri-Gosnet, A.-M.; Renard, J.-P. CMR manganites: Physics, thin films and devices. *J. Appl. Phys.* **2003**, *36*, R127. [[CrossRef](#)]
49. Ohring, M. *Materials Science of Thin Films: Deposition & Structure*; Elsevier: Amsterdam, The Netherlands, 2001.
50. Kodama, R.H. Magnetic nanoparticles. *JMMM* **1999**, *200*, 359–372. [[CrossRef](#)]
51. Arbuzova, T.I.; Gizhevskii, B.A.; Naumov, S.V.; Korolev, A.V.; Arbuzov, V.L.; Shal'nov, K.V.; Druzhkov, A.P. Temporal changes in magnetic properties of high-density CuO nanoceramics. *JMMM* **2003**, *258*, 342–344. [[CrossRef](#)]
52. Osipov, V.V.; Viglin, N.A.; Kochev, V.; Samokhvalov, A.A. Microwave absorption at a junction between the ferromagnetic semiconductor HgCr₂Se₄. *JETP Lett.* **1990**, *52*, 386–389.
53. Borukhovich, A.S.; Viglin, N.A.; Osipov, V.V. Spin-polarized transport and submillimetric microwave spectroscopy of solids. *Phys. Solid State* **2002**, *44*, 938–945. [[CrossRef](#)]
54. Watts, S.M.; van Wee, B.J. A solid state paramagnetic maser device driven by electron spin injection. *Phys. Rev. Lett.* **2006**, *97*, 116601. [[CrossRef](#)] [[PubMed](#)]
55. Viglin, N.A.; Ustinov, V.V.; Osipov, V.V. Spin injection maser. *JETP Lett.* **2007**, *86*, 193–196. [[CrossRef](#)]
56. Viglin, N.A.; Ustinov, V.V. Solid-State Conduction-Electron Maser. Russian Federation patent No 2007126305, 10 July 2007. (In Russian). Available online: https://rusneb.ru/catalog/000224_000128_0002351045_20090327_C1_RU/ (accessed on 10 September 2022).
57. Osipov, V.V.; Viglin, N.A. Spin injection and spin transport in a ferromagnet-semiconductor junction: Microwave emission and absorption. *J. Commun. Technol. Electron.* **2003**, *48*, 548–558.

58. Viglin, N.A.; Osipov, V.V.; Samokhvalov, A.A.; Naumov, S.V.; Borukhovich, A.S.; Denisov, O.F. Heterostructure Heusler alloy $\text{Co}_2\text{MnSn-nSnSb}$: Emission in the millimeter and submillimeter microwave range. *Phys. Low-Dimens. Semicond. Struct.* **2000**, *1–2*, 29–36.
59. Osipov, V.V.; Viglin, N.A.; Samokhvalov, A.A. Investigation of heterostructure “ferromagnetic semiconductor-semiconductor” in the millimeter and submillimeter microwave range. *Phys. Lett. A* **1998**, *247*, 353–359. [[CrossRef](#)]
60. Papaconstatopoulos, D.A.; Pikett, W.E. Tight-binding coherent potential approximation study of ferromagnetic $\text{La}_{2/3}\text{Ba}_{1/3}\text{MnO}_3$. *Phys. Rev. B* **1998**, *57*, 12751. [[CrossRef](#)]
61. Irkhin, V.Y.; Katsnel’son, M.I. Half-metallic ferromagnets. *Physics-Uspokhi* **1994**, *37*, 659–676. [[CrossRef](#)]
62. Fiederling, R.; Keim, M.; Reuscher, G.A.; Ossau, W.; Schmidt, G.; Waag, A.; Molenkamp, L.W. Injection and detection of a spin-polarized current in a light-emitting diode. *Nature* **1999**, *402*, 787–790. [[CrossRef](#)]
63. Ohno, H.; Chiba, A.D.; Matsukura, A.F.; Omiya, T.; Abe, E.; Dietl, T.; Ohtani, K. Electric-field control of ferromagnetism. *Nature* **2000**, *408*, 944–946. [[CrossRef](#)]
64. Bebenin, N.G.; Ustinov, V.V. Inverse spin population near ferromagnet/nonmagnetic semiconductor contact. *JMMM* **2004**, *272*, 1917–1918. [[CrossRef](#)]
65. Samokhvalov, A.A.; Osipov, V.V.; Solin, N.I.; Gunichev, A.F.; Korenblit, I.A.; Galdikas, A.P. Electron-magnon interaction in magnetic semiconductors. *JMMM* **1984**, *46*, 191–198. [[CrossRef](#)]
66. Solin, N.I.; Samokhvalov, A.A. Influence of a strong electric field on microwave absorption in a ferromagnetic semiconductor $\text{Cd}_{1-x}\text{Ag}_x\text{Cr}_2\text{Se}_4$. *Sov. Phys. Solid State* **1976**, *18*, 1226–1227.
67. Samokhvalov, A.A.; Sukhorukov, Y.P. Effect of hot carriers on the Raman spectra of the magnetic semiconductors CdCr_2Se_4 and HgCr_2Se_4 . *JETP Lett.* **1982**, *35*, 212.
68. Akhiezer, A.I.; Bar’Yakhtar, V.G.; Peletminskii, S.V. Coherent amplification of spin waves. *Phys. Lett.* **1963**, *4*, 129–130. [[CrossRef](#)]
69. Auslender, M.I.; Samokhvalov, A.A.; Solin, N.I.; Shumilov, I.Y. Cherenkov interaction of spin waves with charge carriers in the ferromagnetic semiconductor HgCr_2Se_4 . *Sov. Phys. JETP* **1988**, *67*, 2516–2521.
70. Solin, N.I.; Samokhvalov, A.A.; Shumilov, I.Y. Intensification of magnetostatic and spin waves by the drifting charge carriers in a magnetic semiconductor HgCr_2Se_4 . *JETP Lett.* **1987**, *44*, 597–600.
71. Samokhvalov, A.A.; Solin, N.I.; Viglin, N.A.; Kostylev, V.A.; Osipov, V.V.; Babushkin, V.S. Electron-magnon interaction in magnetic semiconductors. *Phys. Status Solidi B* **1992**, *169*, k93–k98. [[CrossRef](#)]
72. Nagaev, E.L. Magnetolectric waves. *Sov. JETP Lett.* **1987**, *45*, 156.
73. Khitun, A.; Nikonov, D.E.; Kang, L.W. Magnetolectric spin wave amplifier for spin wave logic circuits. *J. Appl. Phys.* **2009**, *106*, 123909. [[CrossRef](#)]
74. Solin, N.I.; Naumov, S.V.; Samokhvalov, A.A. Interface phenomena and microwave magnetoresistance in polycrystalline $\text{La}_{1-x}\text{Ca}_x\text{MnO}_3$ lanthanum manganites. *Phys. Solid State* **2000**, *42*, 925–930. [[CrossRef](#)]
75. Solin, N.I.; Ustinov, V.V.; Naumov, S.V. Colossal magnetoresistance of the inhomogeneous ferromagnetic semiconductor HgCr_2Se_4 . *Phys. Solid State* **2008**, *50*, 901–908. [[CrossRef](#)]
76. Mitra, C.; Raychaudhuri, P.; Köbernik, G.; Dörr, K.; Müller, K.H.; Schultz, L.; Pinto, R. P–n diode with hole- and electron-doped lanthanum manganites. *Appl. Phys. Lett.* **2001**, *79*, 2408–2410. [[CrossRef](#)]
77. Kaul, A.R.; Gorbenko, O.Y.; Kamenev, A.A. The role of heteroepitaxy in the development of new thin-film oxide-based functional materials. *Russ. Chem. Rev.* **2004**, *73*, 861–880. [[CrossRef](#)]
78. Sukhorukov, Y.P.; Telegin, A.V.; Gan’shina, E.A.; Loshkareva, N.N.; Kaul, A.R.; Gorbenko, O.Y.; Mel’nikov, O.V.; Vinogradov, A.N. Tunneling of spin-polarized charge carriers in $\text{La}_{0.8}\text{Ag}_{0.1}\text{MnO}_{3+\delta}$ film with variant structure: Magnetotransport and magneto-optical data. *Tech. Phys. Lett.* **2005**, *31*, 484–487. [[CrossRef](#)]
79. Gan’shina, E.; Loshkareva, N.; Sukhorukov, Y.; Mostovshchikova, E.; Vinogradov, A.; Nomerovannaya, L. Optical and magneto-optical spectroscopy of manganites. *JMMM* **2006**, *300*, 62–66. [[CrossRef](#)]
80. Sukhorukov, Y.P.; Gan’shina, E.A.; Belevtsev, B.I.; Loshkareva, N.N.; Vinogradov, A.N.; Rathnayaka, K.D.D.; Naugle, D.G. Giant change in infrared light transmission in $\text{La}_{0.67}\text{Ca}_{0.33}\text{MnO}_3$ film near the Curie temperature. *J. Appl. Phys.* **2002**, *91*, 4403–4408. [[CrossRef](#)]
81. Granovsky, A.; Sukhorukov, Y.; Gan’shina, E.; Telegin, A. Magnetorefractive effect in magnetoresistive materials. In *Magnetophotonics*; Springer: Berlin/Heidelberg, Germany, 2013; pp. 107–133.
82. Loshkareva, N.N.; Solin, N.I.; Sukhorukov, Y.P.; Lobachevskaya, N.I.; Panfilova, E.V. Optical spectroscopy of phase separation in La_xMnO_3 . *Phys. B Condens. Matter* **2001**, *293*, 390–393. [[CrossRef](#)]
83. Sarychev, A.K.; Boyarintsev, S.O.; Rakhmanov, A.L.; Kugel, K.I.; Sukhorukov, Y.P. Collective volume plasmons in manganites with nanoscale phase separation: Simulation of the measured infrared spectra of $\text{La}_{0.7}\text{Ca}_{0.3}\text{MnO}_3$. *Phys. Rev. Lett.* **2011**, *107*, 267401. [[CrossRef](#)]
84. Melnikov, O.V.; Sukhorukov, Y.P.; Telegin, A.V.; Gan’shina, E.A.; Loshkareva, N.N.; Kaul, A.R.; Smoljak, I.B. The evolution of magneto-transport and magneto-optical properties of thin $\text{La}_{0.8}\text{Ag}_{0.1}\text{MnO}_{3+\delta}$ films possessing the in-plane variant structure as a function of the film thickness. *J. Phys. Condens. Matter* **2006**, *18*, 3753. [[CrossRef](#)]
85. Sukhorukov, Y.P.; Gan’shina, E.A.; Kaul, A.R.; Gorbenko, O.Y.; Loshkareva, N.N.; Telegin, A.V.; Kartavtseva, M.S.; Vinogradov, A.N. $\text{Sm}_{0.55}\text{Sr}_{0.45}\text{MnO}_3/\text{Nd}_{0.55}\text{Sr}_{0.45}\text{MnO}_3$ heteroepitaxial structure: Optical and magnetotransport properties. *Tech. Phys.* **2008**, *53*, 716–721. [[CrossRef](#)]

86. Sukhorukov, Y.P.; Telegin, A.V.; Nosov, A.P.; Gan'shina, E.A.; Stepantsov, E.A.; Lombardi, F.; Winkler, D. Magnetorefractive and Kerr effects in the $[\text{La}_{0.67}\text{Ca}_{0.33}\text{MnO}_3/\text{La}_{0.67}\text{Sr}_{0.33}\text{MnO}_3]_n$ superlattices. *Superlattices Microstruct.* **2014**, *75*, 680–691. [CrossRef]
87. Sukhorukov, Y.P.; Loshkareva, N.N.; Gan'shina, E.A.; Kaul, A.R.; Kamenev, A.A.; Gorbenko, O.Y.; Telegin, A.V. Magneto-transmission and magnetoresistance in film manganite/ferrite heterostructures. *Phys. Met. Metallogr.* **2009**, *107*, 579–587. [CrossRef]
88. Kaul, A.R.; Gorbenko, O.Y.; Loshkareva, N.N.; Sukhorukov, Y.P.; Mostovshchikova, E.V. Magnetic lens based on the ferromagnetic manganites with high T_C -superconductor heterostructure. *Phys. Low Dimens. Semicond. Struct.* **2003**, *7*, 124–129.
89. Gorbenko, O.Y.; Kaul, A.R.; Mel'nikov, O.V.; Gan'shina, E.A.; Ganin, A.Y.; Sukhorukov, Y.P.; Mostovshchikova, E.V. Synthetic routes to colossal magnetoresistance manganites thin films containing unstable or highly volatile metal oxides. *Thin Solid Film.* **2007**, *515*, 6395–6401. [CrossRef]
90. Zhao, T.; Scholl, A.; Zavaliche, F.; Lee, K.; Barry, M.; Doran, A.; Ramesh, R. Electrical control of antiferromagnetic domains in multiferroic BiFeO_3 films at room temperature. *Nat. Mater.* **2006**, *5*, 823–829. [CrossRef] [PubMed]
91. Wang, K.F.; Liu, J.M.; Ren, Z.F. Multiferroicity: The coupling between magnetic and polarization orders. *Adv. Phys.* **2009**, *58*, 321–448. [CrossRef]
92. Inoue, M.; Fujikawa, R.; Baryshev, A.; Khanikaev, A.; Lim, P.B.; Uchida, H.; Aktsipetrov, O.; Fedyanin, A.; Murzina, T.; Granovsky, A. Magnetophotonic crystals. *J. Phys. D Appl. Phys.* **2006**, *39*, R151. [CrossRef]
93. Sukhorukov, Y.P.; Gizhevskii, B.A.; Loshkareva, N.N.; Gorbenko, O.Y.; Kaul, A.R.; Telegin, A.V. Infrared modulator. Russian Federation Patent No 2346315, Bull. No 4, 10 February 2009. (In Russian). Available online: https://rusneb.ru/catalog/000224_00128_0002346315_20090210_C1_RU/ (accessed on 2 September 2022).
94. Bessonova, V.A.; Telegin, A.V.; Nosov, A.P.; Patrakov, E.I.; Makarova, M.V.; Sukhorukov, Y.P. Mid-infrared optical response to magnetic field in the $\text{La}_{0.65}\text{Ba}_{0.35}\text{MnO}_3$ film grown by PLD. *JMMM* **2022**, *564*, 170030. [CrossRef]
95. Granovskii, A.B.; Gan'shina, E.A.; Yurasov, A.N.; Boriskina, Y.V.; Yerokhin, S.G.; Khanikaev, A.B.; Inoue, M.; Vinogradov, A.P.; Sukhorukov, Y.P. Magnetorefractive effect in nanostructures, manganites, and magnetophotonic crystals based on these materials. *J. Commun. Technol. Electron.* **2007**, *52*, 1065–1071. [CrossRef]
96. Sukhorukov, Y.P.; Telegin, A.V.; Loshkareva, N.N.; Kaul, A.R.; Gan'shina, E.A. Infrared Modulator. Russian Federation Patent No 88165, Bull. No 30, 27 October 2009. (In Russian). Available online: https://rusneb.ru/catalog/000224_000128_0000088165_20091027_U1_RU/ (accessed on 9 September 2022).
97. Yurasov, A.N.; Boriskina, Y.V.; Gan'shina, E.A.; Granovsky, A.B.; Sukhorukov, Y.P. Magnetorefractive effect in manganites. *Phys. Solid State* **2007**, *49*, 1121–1124. [CrossRef]
98. Sukhorukov, Y.P.; Telegin, A.V.; Gan'shina, E.A. Simultaneous controlling the intensity of reflected and transmitted light in thin films of manganites. *Tech. Phys.* **2021**, *66*, 942–946. [CrossRef]
99. Sukhorukov, Y.P.; Telegin, A.V.; Granovsky, A.B.; Gan'shina, E.A.; Zhukov, A.; Gonzalez, J.; Herranz, G.; Caicedo, J.M.; Yurasov, A.N.; Bessonov, V.D.; et al. Magnetorefractive effect in manganites with a colossal magnetoresistance in the visible spectral region. *JETP* **2012**, *114*, 141–149. [CrossRef]
100. Formisano, F.; Medapalli, R.; Xiao, Y.; Ren, H.; Fullerton, E.E.; Kimel, A.V. Femtosecond magneto-optics of EuO . *JMMM* **2020**, *502*, 166479. [CrossRef]
101. van Kooten, S.C.P.; Springholz, G.; Henriques, A.B. Direct optical probing of ultrafast spin dynamics in a magnetic semiconductor. *Phys. Rev. B* **2022**, *105*, 224427. [CrossRef]
102. Ishihara, S. Photoinduced ultrafast phenomena in correlated electron magnets. *J. Phys. Soc. Jpn.* **2019**, *88*, 072001. [CrossRef]
103. Sukhorukov, Y.P.; Moskvina, A.M.; Loshkareva, N.N.; Smolyak, I.B.; Arkhipov, V.E.; Mukovskii, Y.M.; Shmatok, A.V. Magneto-optical Faraday effect in $\text{La}_{0.7}\text{Sr}_{0.3}\text{MnO}_{3-\delta}$ films. *Tech. Phys.* **2001**, *46*, 778–781. [CrossRef]
104. Park, J.H.; Takagi, H.; Nishimura, K.; Uchida, H.; Inoue, M.; Park, J.H.; Cho, J.K. Magneto-optic spatial light modulators driven by an electric field. *J. Appl. Phys.* **2003**, *93*, 8525–8527. [CrossRef]
105. Park, J.H.; Sung, I.K.; Cho, J.K.; Nishimura, K.; Uchida, H.; Inoue, M. Flat-surface pixel for magneto-optic spatial light modulator. *IEEE Trans. Magn.* **2003**, *39*, 3169–3171. [CrossRef]
106. Park, J.H.; Kim, J.H.; Cho, J.K.; Nishimura, K.; Uchida, H.; Inoue, M. An optical micro-magnetic display. *JMMM* **2004**, *272*, 2260–2262. [CrossRef]
107. Bukharaev, A.A.; Zvezdin, A.K.; Pyatakov, A.P.; Fetisov, Y.K. Straintronics: A new trend in micro- and nanoelectronics and materials science. *Physics-Uspokhi* **2018**, *61*, 1175. [CrossRef]
108. Sukhorukov, Y.P.; Telegin, A.V.; Bebenin, N.G.; Nosov, A.P.; Bessonov, V.D.; Buchkevich, A.A. Strain-magneto-optics of a magnetostrictive ferrimagnetic CoFe_2O_4 . *Solid State Commun.* **2017**, *263*, 27–30. [CrossRef]
109. Sukhorukov, Y.; Telegin, A.; Bebenin, N.; Bessonov, V.; Naumov, S.; Shishkin, D.; Nosov, A. Strain-magneto-optics in single crystals of CoFe_2O_4 . *Magnetochemistry* **2022**, *8*, 135. [CrossRef]
110. Telegin, A.V.; Sukhorukov, Y.P.; Bebenin, N.G. Anisotropic magnetoabsorption of light in cobalt ferrite and its correlation with magnetostriction. *JETP* **2020**, *131*, 970–975. [CrossRef]
111. Sukhorukov, Y.P.; Telegin, A.V.; Bebenin, N.G.; Nosov, A.P.; Bessonov, V.D.; Buchkevich, A.A.; Patrakov, E.I. Magnetoreflexion and magnetostriction in ferrimagnetic spinels CoFe_2O_4 . *J. Exp. Theor. Phys.* **2018**, *126*, 106–114. [CrossRef]
112. Nasirpour, F.; Nogaret, A. (Eds.) *Nanomagnetism and Spintronics: Fabrication, Materials, Characterization and Applications*; World Scientific: Singapore, 2010; 400p.

113. Zimnyakova, P.E.; Ignatyeva, D.O.; Karki, D.; Voronov, A.A.; Shaposhnikov, A.N.; Berzhansky, V.N.; Belotelov, V.I. Two-dimensional array of iron-garnet nanocylinders supporting localized and lattice modes for the broadband boosted magneto-optics. *Nanophotonics* **2022**, *11*, 119–127. [CrossRef]
114. Omelyanchik, A.; Villa, S.; Singh, G.; Rodionova, V.; Laureti, S.; Canepa, F.; Peddis, D. Magnetic properties of Bi-magnetic core/shell nanoparticles: The case of thin shells. *Magnetochemistry* **2021**, *7*, 146. [CrossRef]
115. Gupta, A.; Zhang, R.; Kumar, P.; Kumar, V.; Kumar, A. Nano-structured dilute magnetic semiconductors for efficient spintronics at room temperature. *Magnetochemistry* **2020**, *6*, 15. [CrossRef]
116. Dmitriev, A.I.; Talantsev, A.D.; Zaitsev, S.V.; Koplak, O.V.; Morgunov, R.B. Nano-and heterostructures of magnetic semiconductors for spintronics. *Russ. Chem. Bull.* **2011**, *60*, 1051–1057. [CrossRef]
117. Silva, A.S.; Guimarães, É.V.; Sales, T.O.; Silva, W.S.; Batista, E.A.; Jacinto, C.; Silva, R.S. Nanostructured magnetic semiconductors. In *Fundamentals of Low Dimensional Magnets*; CRC Press: Boca Raton, FL, USA, 2022; pp. 23–39.
118. Kotnala, R.K.; Shah, J. Ferrite materials: Nano to spintronics regime. In *Handbook of Magnetic Materials*; Elsevier: Amsterdam, The Netherlands, 2015; Volume 23, pp. 291–379. [CrossRef]
119. Loshkareva, N.N.; Sukhorukov, Y.P.; Gizhevskii, B.A.; Naumov, S.V.; Samokhvalov, A.A.; Moskvina, A.S.; Belykh, T.A. Polar-center phase nuclei in He⁺-irradiated CuO single crystals. *Phys. Solid State* **1998**, *40*, 383–388. [CrossRef]
120. Lin, H.H.; Wang, C.Y.; Shih, H.C.; Chen, J.M.; Hsieh, C.T. Characterizing well-ordered CuO nanofibrils synthesized through gas-solid reactions. *J. Appl. Phys.* **2004**, *95*, 5889–5895. [CrossRef]
121. Baru, V.G.; Volkenshtein, F.F. *Influence of Irradiation on the Surface Properties of Semiconductors*; Nauka: Moscow, Russia, 1978.
122. Yermakov, A.Y.; Feduschak, T.A.; Sedoi, V.S.; Uimin, M.A.; Mysik, A.A. Magneto-modified catalyst on the base of nanocrystalline CuO. *JMMM* **2004**, *272*, 2445–2447. [CrossRef]
123. Morales, J.; Sánchez, L.; Martín, F.; Ramos-Barrado, J.R.; Sánchez, M. Nanostructured CuO thin film electrodes prepared by spray pyrolysis: A simple method for enhancing the electrochemical performance of CuO in lithium cells. *Electrochim. Acta* **2004**, *49*, 4589–4597. [CrossRef]
124. Wei, Q.; Luo, W.D.; Liao, B.; Liu, Y.; Wang, G. Giant capacitance effect and physical model of nano crystalline CuO–BaTiO₃ semiconductor as a CO₂ gas sensor. *J. Appl. Phys.* **2000**, *88*, 4818–4824. [CrossRef]
125. Pilyugin, V.P.; Gizhevskii, B.A.; Patselov, A.M.; Chernyshev, E.G.; Lisin, V.L. Plastic deformation Chamber at Low Temperatures. Russian Federation patent No 61882, Bull. No 7, 10 March 2007. Available online: https://rusneb.ru/catalog/000224_000128_000061882_20070310_U1_RU/ (accessed on 11 September 2022).
126. Pilyugin, V.P.; Chernyshev, E.G.; Patselov, A.M.; Gizhevskii, B.A. High Pressure Chamber for Spectroscopic Analysis. Russian Federation Patent No 60727, Bull. No 3, 27 January 2007. (In Russian). Available online: https://rusneb.ru/catalog/000224_000128_0000060727_20070127_U1_RU/ (accessed on 11 September 2022).
127. Arbuzova, T.I.; Voronin, V.I.; Gizhevskii, B.A.; Naumov, S.V.; Arbuzov, V.L. An inhomogeneous paramagnetic state of the LaMnO_{3+δ} nanoceramics prepared by shock-wave loading. *Phys. Solid State* **2010**, *52*, 1217–1226. [CrossRef]
128. Gizhevskii, B.A.; Galakhov, V.R.; Kozlov, E.A. Effects of shock-wave loading in oxides. *Petrology* **2012**, *20*, 317–330. [CrossRef]
129. Gizhevskii, B.A.; Sukhorukov, Y.P.; Moskvina, A.S.; Loshkareva, N.N.; Mostovshchikova, E.V.; Ermakov, A.E.; Gaviko, V.S. Anomalies in the optical properties of nanocrystalline copper oxides CuO and Cu₂O near the fundamental absorption edge. *JETP* **2006**, *102*, 297–302. [CrossRef]
130. Krynetskii, I.B.; Gizhevskii, B.A.; Naumov, S.V.; Kozlov, E.A. Size effect of the thermal expansion of nanostructural copper oxide. *Phys. Solid State* **2008**, *50*, 756–758. [CrossRef]
131. Vykhodets, V.B.; Vykhodets, E.V.; Gizhevskii, B.A.; Zakharov, R.G.; Kozlov, E.A.; Kurennykh, T.E.; Petrova, S.A.; Trakhtenberg, I.S.; Fishman, A.Y. Grain boundary self-diffusion of tracer ¹⁸O atoms in nanocrystalline oxide LaMnO_{3+δ}. *JETP Lett.* **2008**, *87*, 115–119. [CrossRef]
132. Arbuzova, T.I.; Naumov, S.V.; Kozlov, E.A.; Arbuzov, V.L.; Shal'nov, K.V.; Gizhevskii, B.A.; Voronin, V.I. Influence of structural defects on magnetic properties of the submicrometer ceramic Mn₃O₄. *JETP* **2006**, *102*, 931–937. [CrossRef]
133. Gizhevskii, B.A.; Kozlov, E.A.; Ermakov, A.E.; Lukin, N.V.; Naumov, S.V.; Samokhvalov, A.A. Microstructure of CuO after shock-loading and milling. *Phys. Met. Metallogr.* **2001**, *92*, 153–157.
134. Druzhkov, A.P.; Gizhevskii, B.A.; Arbuzov, V.L.; Kozlov, E.A.; Shal'nov, K.V.; Naumov, S.V.; Perminov, D.A. Electronic and structural properties of micro- and nanometre-sized crystalline copper monoxide ceramics investigated by positron annihilation. *J. Phys. Condens. Matter* **2002**, *14*, 7981. [CrossRef]
135. Gizhevskii, B.A.; Sukhorukov, Y.P.; Gan'shina, E.A.; Loshkareva, N.N.; Telegin, A.V.; Lobachevskaya, N.I.; Gaviko, V.S.; Pilyugin, V.P. Optical and magneto-optical properties of nanostructured yttrium iron garnet. *Phys. Solid State* **2009**, *51*, 1836–1842. [CrossRef]
136. Makhnev, A.A.; Gizhevskii, B.A.; Nomerovannaya, L.V. Optical spectra of nanoceramics of yttrium-iron garnet Y₃Fe₅O₁₂ obtained by the method of intense plastic deformation. *JETP Lett.* **2010**, *91*, 79–82. [CrossRef]
137. Falkovskaya, L.D.; Fishman, A.Y.; Mitrofanov, V.Y.; Ivanov, M.A. Random fields in disordered magnetics with Jahn-Teller ions. In Proceedings of the Fifth International Conference on Mathematical Modeling and Computer Simulations of Materials Technologies, Ariel, Israel, 21–23 July 2015; pp. 1–202.
138. Agnihotri, O.P.; Gupta, B.K. *Solar Selective Surfaces*; Wiley-Interscience: New York, NY, USA, 1981; 232p.
139. Tesfamichael, T.; Hoel, A.; Wäckelgard, E.; Niklasson, G.A.; Gunde, M.K.; Orel, Z.C. Optical characterization and modeling of black pigments used in thickness-sensitive solar-selective absorbing paints. *Sol. Energy* **2001**, *69*, 35–43. [CrossRef]

140. Van Buskirk, O.R. Solar Selective Surfaces. U.S. Patent No 4310596, 12 January 1982. Available online: <https://www.freepatentsonline.com/4310596.html> (accessed on 11 September 2022).
141. Karlsson, B.; Ribbing, C.G.; Roos, A.; Valkonen, E.; Karlsson, T. Optical properties of some metal oxides in solar absorbers. *Phys. Scr.* **1982**, *25*, 826. [[CrossRef](#)]
142. Sukhorukov, Y.P.; Gizhevskii, B.A.; Mostovshchikova, E.V.; Yermakov, A.Y.; Tugushev, S.N.; Kozlov, E.A. Nanocrystalline copper oxide for selective solar energy absorbers. *Tech. Phys. Lett.* **2006**, *32*, 132–135. [[CrossRef](#)]
143. Ovchinnikov, S.G.; Gizhevskii, B.A.; Sukhorukov, Y.P.; Ermakov, A.E.; Uimin, M.A.; Kozlov, E.A.; Bagazeev, A.V. Specific features of the electronic structure and optical spectra of nanoparticles with strong electron correlations. *Phys. Solid State* **2007**, *49*, 1116–1120. [[CrossRef](#)]
144. Shabatina, T.I.; Vernaya, O.I.; Shabatin, V.P.; Melnikov, M.Y. Magnetic nanoparticles for biomedical purposes: Modern trends and prospects. *Magnetochemistry* **2020**, *6*, 30. [[CrossRef](#)]
145. Rempel, A.A. Nanotechnologies. Properties and applications of nanostructured materials. *Russ. Chem. Rev.* **2007**, *76*, 435. [[CrossRef](#)]
146. Simovski, C.; Tretyakov, S. *An Introduction to Metamaterials and Nanophotonics*; Cambridge University Press: Cambridge, UK, 2020.
147. Kumar, C.S. *Magnetic Nanomaterials*; John Wiley & Sons: Hoboken, NJ, USA, 2009.
148. Kharat, P.B.; Somvanshi, S.B.; Jadhav, K.M. Multifunctional magnetic nano-platforms for advanced biomedical applications: A brief review. *J. Phys. Conf. Ser.* **2020**, *1644*, 012036. [[CrossRef](#)]
149. Ishii, T.; Yamakawa, H.; Kanaki, T.; Miyamoto, T.; Kida, N.; Okamoto, H.; Ohya, S. Ultrafast magnetization modulation induced by the electric field component of a terahertz pulse in a ferromagnetic-semiconductor thin film. *Sci. Rep.* **2018**, *8*, 1–6. [[CrossRef](#)] [[PubMed](#)]
150. Kimel, A.V.; Kalashnikova, A.M.; Pogrebna, A.; Zvezdin, A.K. Fundamentals and perspectives of ultrafast photoferroic recording. *Phys. Rep.* **2020**, *852*, 1–46. [[CrossRef](#)]
151. Telegin, A.V.; Bebenin, N.G.; Zainullina, R.I.; Mostovshchikova, E.V.; Viglin, N.A.; Gan'shina, E.A.; Zykov, G.S.; Fedorov, V.A.; Menshchikova, T.K.; Buchkevich, A.A. Optical and magneto-optical effects in $\text{Hg}_{1-x}\text{Cd}_x\text{Cr}_2\text{Se}_4$ ($0 \leq x \leq 1$) single crystals. *JETP* **2015**, *121*, 437–445. [[CrossRef](#)]
152. Huisman, T.J.; Mikhaylovskiy, R.V.; Telegin, A.V.; Sukhorukov, Y.P.; Granovsky, A.B.; Naumov, S.V.; Rasing, T.; Kimel, A.V. Terahertz magneto-optics in the ferromagnetic semiconductor $\text{HgCdCr}_2\text{Se}_4$. *Appl. Phys. Lett.* **2015**, *106*, 132411. [[CrossRef](#)]
153. Barsaume, S.; Telegin, A.V.; Sukhorukov, Y.P.; Stavrias, N.; Fedorov, V.A.; Menshchikova, T.K.; Rasing, T.; Kimel, A.V. Static and time-resolved mid-infrared spectroscopy of $\text{Hg}_{0.95}\text{Cd}_{0.05}\text{Cr}_2\text{Se}_4$ spinel. *J. Phys. Condens. Matter* **2017**, *29*, 325502–325508. [[CrossRef](#)] [[PubMed](#)]
154. Pogrebna, A.; Barsaume, S.; Subkhangulov, R.R.; Telegin, A.V.; Sukhorukov, Y.P.; Chzhan, A.V.; Rasing, T.; Kimel, A.V. Spectral tunability of laser-induced spin dynamics in the ferromagnetic semiconductor CdCr_2Se_4 . *Phys. Rev. B* **2018**, *98*, 214427–214433. [[CrossRef](#)]